

Elsevier Editorial System(tm) for Composites Part B
Manuscript Draft

Manuscript Number: JCOMB-D-13-00591R1

Title: Blast performance of a sacrificial cladding with composite tubes for protection of civil engineering structures

Article Type: Special Issue: Damage Mechanics

Keywords: A Polymer-matrix composites
B Impact behaviour
C Numerical analysis
D Mechanical testing

Corresponding Author: Prof. Wim Van Paepegem, PhD

Corresponding Author's Institution: Ghent University

First Author: Wim Van Paepegem, PhD

Order of Authors: Wim Van Paepegem, PhD; Sivakumar Palanivelu; Joris Degrieck; John Vantomme; Bruno Reymen; Dimitris Kakogiannis; Danny Van Hemelrijck; Jan Wastiels

Abstract: Crushing of composite tubes under impact loading has been studied very intensively over the last few decades. On the contrary, the energy absorption of composite tubes under blast loading is much less studied, and very limited public literature is available. This paper presents the experimental testing of a sacrificial cladding structure, composed of glass/polyester tubes, under blast loading. The composite tubes show stable and progressive crushing and considerably lower the peak force transferred to the non-sacrificial structure.

BLAST PERFORMANCE OF A SACRIFICIAL CLADDING WITH COMPOSITE TUBES FOR PROTECTION OF CIVIL ENGINEERING STRUCTURES

W. Van Paepegem^{1*}, S. Palanivelu¹, J. Degrieck¹, J. Vantomme², B. Reymen², D. Kakogiannis², D. Van Hemelrijck³, J. Wastiels³

¹ Department of Materials Science and Engineering, Ghent University, Technologiepark-Zwijnaarde 903, 9052 Zwijnaarde, Belgium

² Royal Military Academy, Civil and Materials Engineering Department, Building G, Level 0, 8 Av. Hobbema B-1000, Brussels, Belgium

³ Department of Mechanics of Materials and Constructions, Vrije Universiteit Brussel, Pleinlaan 2 B-1050 Brussels, Belgium

*Wim.VanPaepegem@UGent.be

Abstract

Crushing of composite tubes under impact loading has been studied very intensively over the last few decades. On the contrary, the energy absorption of composite tubes under blast loading is much less studied, and very limited public literature is available. This paper presents the experimental testing of a sacrificial cladding structure, composed of glass/polyester tubes, under blast loading. The composite tubes show stable and progressive crushing and the peak force transferred to the non-sacrificial structure is compared for different configurations of the composite tubes. The results also show that the diffraction of the pressure wave and the skin panel that distributes the blast pressure are critical issues in the set-up of the experiments.

Keywords:

A Polymer-matrix composites

B Impact behaviour

C Numerical analysis

D Mechanical testing

1 Introduction

When civil engineering structures are subjected to blast loading, the failure of the critical load bearing members such as beams, pillars, columns etc., and its debris can cause major human casualties. Hence a preventive solution is needed to safeguard those civil engineering structures. Out of many proposed solutions, the concept of sacrificial claddings has attracted a lot of attention [1-6] in terms of its functionality and its predictable behaviour. Any sacrificial cladding structure can have two layers (an inner core and outer skin panels). The function of the skin panel is to distribute the blast pressure more evenly to the inner core which deforms progressively and absorbs most of the energy from the blast load, so that the main load bearing members of the civil engineering structures will be safeguarded.

In case of impulsive blast loading on civil engineering structures and sacrificial cladding structures, the positive duration of the blast load will be much shorter than the natural period of the structure. In order to protect civil engineering structures from such a blast load, the proposed sacrificial cladding structure should be mounted or assembled in front of those structures. During a blast loading the sacrificial cladding structure will receive a high load (p_0) - short duration impulse (Figure 1). The function of the sacrificial cladding structure as a whole is to change the force-time distribution from a high load - short duration impulse to a low load - long duration impulse (Figure 1). To avoid permanent damage in the main structure (non-sacrificial structure), the failure load of the sacrificial cladding structure (F_{max}) should be kept well below the minimum elastic capacity of the non-sacrificial cladding structure. By doing so, the transferred peak force to the non-sacrificial structure can be minimised [7]. The mechanism by which a sacrificial cladding structure does this, is absorbing energy through elastic, plastic or brittle deformations. During this process the conservation of (linear)

1 momentum should be satisfied. Furthermore, the blast loads typically produce very high strain
2 rates. The strain rate and the corresponding strain hardening alter the dynamic mechanical
3 properties of the target structures (sacrificial cladding structure). Hence, these factors should
4 be thoroughly studied and taken into account while deploying a material for the inner core of
5 a sacrificial cladding structure.
6
7
8
9
10

11 This contribution focuses on a sacrificial cladding structure with the core consisting of an
12 array of composite tubes which should be responsible for the major energy absorption from
13 the blast. Over the past years, a lot of research has been done on crushing of tubes for energy
14 absorption [8-20]. The authors themselves have studied the energy absorption of a single
15 composite tube under axial impact and air blast loading [21-26]. Those models for crushing
16 have been thoroughly validated by small-scale drop weight tests and blast tests in a bunker.
17 The purpose of the research presented here, is to validate the proof-of-concept with larger-
18 scale air blast tests on a representative sacrificial cladding structure, composed of pultruded
19 glass/polyester composite tubes as core material and sandwich composite skin plates.
20
21
22
23
24
25
26
27
28
29
30
31
32
33
34
35

36 **2. Behaviour of the pultruded glass/polyester tubes under varying strain rate**

37 In a first step, the strain rate sensitivity of the pultruded glass/polyester tubes is investigated.
38 This step is very important, because many insights from quasi-static and impact loading can
39 be transferred directly to the blast loading tests, if the strain rate sensitivity is limited.
40
41
42
43
44
45

46 The material, architecture and dimensional parameters of the composite tubes for the blast
47 loading are the same as for the quasi-static and impact testing, previously conducted by the
48 authors [21-26]. The tubes consist of pultruded unidirectional glass fibres in a polyester
49 matrix. The cross-section is circular or square and wall thicknesses are chosen such to assure
50 stable and progressive crushing. The effect of filling the hollow tubes with foam, has been
51 studied in quasi-static and impact loading [23] and shows that foam filling is only beneficial if
52
53
54
55
56
57
58
59
60
61
62
63
64
65

1 the density of the foam is sufficiently low. If the foam density is too high, the inward bending
2 of the petals is prevented and the progressive delamination is suppressed. This results in a
3 smaller specific energy absorption (SEA), compared to hollow tubes.
4
5
6
7
8

9 **2.1. Consistency of deformation patterns**

10
11
12 In quasi-static and impact loading, it was observed that the inner and outer petals were formed
13 due to the circumferential delamination and, consequently, axial cracks were formed parallel
14 to the axis of the tube. The uniform geometry of the circular tube facilitated to form more
15 axial cracks and, thus, more petals were formed. The major amount of impact energy was
16 absorbed due to the increasing number of longitudinal cracks and subsequent bending of the
17 laminae [21].
18
19
20
21
22
23
24
25
26
27
28
29
30

31 To conduct close-range free air blast tests on a single composite tube, a special laboratory test
32 set-up was designed and manufactured (Figure 2). The spherical explosive (typically 20-50 g)
33 is hanging above the test set-up. After detonation, a spherical shock wave propagates towards
34 the skin plate, that transfers the blast pressure to a single composite tube underneath it. That
35 composite tube is progressively crushed and a side cover tube prevents the blast pressure from
36 acting sideways on the composite tube during deformation. Different parameters have been
37 varied in the experiments, such as spherical explosive (C4) mass, stand-off distance, area of
38 skin plate and mass of the skin plate. The incident angle for all tests was zero.
39
40
41
42
43
44
45
46
47
48
49
50
51
52

53 During the air blast tests, the following parameters were measured:

- 54 • the incident pressure (with a blast pencil)
- 55
- 56 • the reflected pressure at the surface of the skin plate (with a pressure sensor)
- 57
- 58
- 59
- 60
- 61
- 62
- 63
- 64
- 65

- the accelerations of the skin plate (with an accelerometer), and by integration, the velocity and displacement of the skin plate,
- the transferred load to the "non-sacrificial structure" (by a load cell below the composite tube),
- digital high speed imaging of the blast event.

The deformation patterns of the circular cross sectional composite tubes are shown in Figure 3. It can be noticed that the crushing failure mechanisms of these tubes are the same as for the quasi-static testing results.

Further, it has been investigated if the same conclusion applies for different thickness/diameter ratios. To that purpose, thicker commercially available pultruded glass polyester composite tubes (M/s Exel composites, Belgium) have been tested. The deformation patterns of these tubes under blast loading are presented in Figure 4 and are again in accordance with static deformation patterns.

Furthermore, the same finding was also validated for contact blast loading using a suspended pendulum test set-up which was developed in collaboration with Prof. Gerald Nurick from University of Cape town, South Africa (Figure 5(a)) [27]. Tests have been conducted on this pendulum set-up with different sizes of cylindrical charge masses and with different striker masses. As an example, the deformation patterns of the tubes subjected to contact blast loading are given in Figure 5(b). The failure mechanism and the patterns of these tubes are the same when compared to quasi-static experimental results. Hence, it can be concluded that the failure mechanisms and the failure patterns of these tubes (unidirectional glass polyester composite tubes) seems to remain identical irrespective of the strain rate.

2.2. Strain rate insensitivity

1
2 The pultruded composite tubes show strain rate insensitivity over the complete range of
3
4 loading from quasi-static testing till free air blast loading.
5
6

7 Figure 6 shows the comparison of the force-deformation curves of composite tubes with
8
9 triggering type 1 (45° chamfering) and triggering type 2 (tulip triggering) for quasi-static,
10
11 impact and blast loading conditions. Figure 6(a) shows the average force-deformation curves
12
13 (from 4 tests of each type) of circular cross sectional composite tubes with triggering type 1.
14
15 The quasi-static tests were performed with a cross head displacement of 10 mm/min; impact
16
17 tests were performed for an initial impact velocity of 6.0 m/s with an impactor mass of 7.6 kg;
18
19 and the free air blast tests were performed for 40g of C4 with stand-off distance of 30 cm. It
20
21 can be noticed that the average peak crush load of these cases is very close to each other
22
23 (deviation of less than 10 % of the peak crush loads). A similar result was also observed for
24
25 triggering type 2 (refer Figure 6(b)). Based on the results of the experiments presented hereto,
26
27 it can be concluded that for uni-directional fibre orientation the effect of strain-rate on the
28
29 peak crush load is negligible. Similar results have also been reported for glass polyester
30
31 pultruded composite tubes in ref [28].
32
33
34
35
36
37
38
39
40

41 Due to the same deformation patterns in all loading conditions (quasi-static, impact and blast)
42
43 and the absence of strain-rate effects on the peak crush load, the influence of the triggering
44
45 mechanism on the force-deformation curves remains the same when compared to quasi-static
46
47 tests (Figure 6(a) and 6(b)). Unlike for the quasi-static tests and impact tests, the crush load of
48
49 the tubes for blast load decreased after the peak load. This was due to the short duration of the
50
51 loading and a lower skin plate mass (compared with quasi-static and impact loading) resulting
52
53 in a lower deformation length.
54
55
56
57
58
59
60
61
62
63
64
65

2.3. Simulation of the experimental set-up

1
2 In order to understand the efficiency of the composite tubes for energy absorption under blast
3
4 loading, the impulse delivered to the top face of the skin plate (reflected impulse) and the
5
6 corresponding transferred impulse at the bottom of the composite tube to the non-sacrificial
7
8 member (integration of measured force-time history at the bottom of the composite tube) were
9
10 compared. Approximately 30 % difference between the reflected impulse and the transferred
11
12 impulse was observed in all cases, and hence, the linear momentum was not conserved for any
13
14 of the cases. This result is unexpected, because a sacrificial cladding structure cannot prevent
15
16 the impulse of the blast being transferred onto the structure upon which it is mounted, rather it
17
18 changes the force-time distribution from a high load, short duration impulse to a low load,
19
20 long duration impulse and thereby avoiding or reducing the damage to the nonsacrificial
21
22 structure upon which it is mounted.
23
24
25
26
27

28
29 In order to understand the large difference between reflected and transferred impulse, the
30
31 whole experimental set-up was also modelled in the finite element code Autodyn. In order to
32
33 reduce the computational time the blast simulation for the discussed experimental set-up was
34
35 done in two stages. The first stage is the analysis of the detonation of the C4 explosive and
36
37 propagation of the pressure waves. In Autodyn v12.1 this analysis can be done using a 2D
38
39 approach.
40
41
42

43
44 The detonation of the C4 explosive was modelled with a wedge (Figure 7). Accordingly 1000
45
46 grids (elements) were chosen along the radial axis in the air medium. The air and C4 were
47
48 modelled using *multi-material Euler formulation*. The initiation, detonation and the expansion
49
50 of C4 was modelled using the *Jones-Wilkins-Lee (JWL) Equation of state (EOS)*.
51
52

53
54 The spherical charge of 20g C4 was modelled with an equivalent radius of 14 mm in the 2D
55
56 model. Similarly, the wedge area filled with ambient air was modelled using the ideal gas
57
58 equation.
59
60
61

1 In order to compare the incident blast parameters, the results from the Hydrocodes calculation
2 was compared with *ConWep* data for the same input parameters (20 g C4 and 30 cm stand-off
3 distance). Figure 8 shows a comparison of the incident blast parameters (arrival time, peak
4 incident pressure and the positive phase duration) from Autodyn, *ConWep* and experimentally
5 measured data. For the simplification only the positive phase of the pressure-time history is
6 considered.
7
8
9
10
11
12
13
14
15
16

17 The magnitude of peak incident overpressure from the experimental measurement and the
18 calculated value from Autodyn were very close to the *ConWep* predicted data (923 kPa, 920
19 kPa and 898.7 kPa from the experiment, Autodyn and *ConWep* respectively). Furthermore,
20 there was a good correlation observed for arrival time and positive phase duration between the
21 experimentally measured data (0.121 ms and 0.378 ms respectively) and Autodyn simulated
22 values (0.126 ms and 0.37 ms respectively). However, the predicted time of arrival and the
23 positive phase duration from *ConWep* showed longer durations (0.162 ms and 0.6941 ms for
24 arrival time and positive duration of the blast respectively).
25
26
27
28
29
30
31
32
33
34
35

36 The second part deals with the propagation of blast pressure in a 3D computational model
37 using 2D data. The remapping option of Autodyn provides this feature.
38
39
40

41 The air was modelled as a rectilinear box with Eulerian grid. The boundary of the air model
42 was chosen to have adequate air space in all directions from the centre of detonation. The
43 dimensional details and the 3D computational modelling of the experimental set-up are shown
44 in Figure 9.
45
46
47
48
49
50

51 On the rectilinear air flow domain, the “flow-out” boundary condition was assigned to all
52 boundary planes of the 3D domain except the base plane, which represented the ground
53 surface. This boundary condition is needed to simulate the reflection of pressure waves from
54 the ground surface. The interaction of blast pressure waves with the aluminium skin plate and
55
56
57
58
59
60
61
62
63
64
65

1 the side tube was defined by a fully coupled feature available in Autodyn v12.1. The fully
2 coupled algorithm allows the Lagrange and the Euler-FCT (Flux Corrected Transport)
3 formulation to be coupled in a single problem. With help of this approach a high order
4 solution is computed wherever possible in the flow field. This coupled algorithm
5 automatically detects the interfacing faces of the aluminium skin plate, the side cover tube and
6 the rigid support. These interfacing faces act as a physical constraint to the fluid domain.
7 Consequently, the resultant shock from the pressure waves on the aluminium skin plate will
8 be transferred to the test specimen.
9

10 The magnitude of the reflected pressure wave was calculated at the air grid which was closer
11 to the top and bottom faces of the skin plates (1 μm away from the faces). In order to study
12 the effect of the grid size on the blast parameters, a mesh sensitivity study was conducted for
13 the air model with the aluminium skin plate (ϕ 200 mm; 1.0 kg) with the following grid sizes :
14 0.25 mm, 0.5 mm, 1 mm, 5mm, 10 mm and 15 mm. Only for the smallest element sizes (0.25
15 mm and 0.5 mm) the magnitude of the peak reflected pressures (4849 kPa and 4745 kPa
16 respectively) was very close to the ConWep value (4755 kPa). An element size of 0.25 mm
17 was used for all the analyses.
18

19 The clearing of reflected pressure waves and the subsequent diffraction phenomenon can be
20 explained by investigating the propagation and interaction of blast pressure waves with
21 respect to time. As an example, the 30 cm stand-off distance case is discussed here. Figure 10
22 shows the interaction of the pressure waves (at the mid-plane representing $X = 0$ and $Z = 0$)
23 with the top and bottom faces of the aluminium skin plate. These figures show a
24 chronological event of interaction and diffraction of the pressure waves around the edges of
25 the aluminium skin plate. As we have mentioned earlier the remapping of the 2D blast wave
26 was fed into the 3D computational model. After remapping, the analysis was started when the
27 pressure reached 0.25 mm above the top face of the skin plate (this corresponds to time $t = 0$
28
29
30
31
32
33
34
35
36
37
38
39
40
41
42
43
44
45
46
47
48
49
50
51
52
53
54
55
56
57
58
59
60
61
62
63
64
65

1 ms). The magnitude of the pressure wave increased suddenly when the incident pressure was
2 obstructed by the top face of the skin plate. Due to the spherical wave front, a higher
3 magnitude was observed at the centre of the top face of the skin plate. This event started after
4 approximately 0.8 μ s at the centre of the top face of the plate and it lasted for approximately
5 1.9 μ s. After that the amplitude reduced exponentially. During this period a significant
6 amount of pressure waves (especially the pressure wave at the periphery of the top face of the
7 skin plate) diffracted around the top edge of the skin plate (clearing phenomenon). Due to this
8 clearing the magnitude of the reflected pressure wave was reduced significantly in a short
9 time.
10

11 The later time increments of the analysis showed the interaction of ground reflected pressure
12 with the skin plate. As an example, the numerical evidence of the interaction of pressure
13 waves from the ground reflection for 30 cm stand-off distance is shown in Figure 11.
14

15 The impulse from the diffraction and ground reflection was opposite to the direction of the
16 reflected impulse at the top face of the skin plate. Therefore, the resultant impulse imparted to
17 the top skin plate and the corresponding transferred impulse (I_{trans}) to the solid copper tube
18 was equal to the difference between the reflected impulse and the combined impulse from the
19 diffraction and ground reflection ($I_{resultant} = I_{ref} - I_{diffraction} - I_{ground\ reflection}$). The calculated
20 combined impulse from diffraction and ground reflection at the bottom face of the skin plate
21 was approximately 31% and 29.4% of the total reflected impulse at the top face of the
22 aluminium skin plate (ϕ 250 mm; 1.0 kg) for 30 cm and 15 cm stand-off distance respectively.
23 Now, these values (31% and 29.4%) can be compared with the average difference in impulse
24 ($\Delta I = I_{refl} - I_{trans}$) observed during the experimental testing. The average difference in the
25 experimental impulse varied from a minimum of 28% to a maximum of 33 %. From the
26 results of the above analyses it can be concluded that approximately 30% of the total impulse
27 was lost due to the diffraction and ground reflection phenomena.
28
29
30
31
32
33
34
35
36
37
38
39
40
41
42
43
44
45
46
47
48
49
50
51
52
53
54
55
56
57
58
59
60
61
62
63
64
65

1 The outcome of the numerical simulations was also confirmed by the high speed images in
2 Figure 12, which show a very quick clearing of the pressure waves around the edges of the
3 top skin plate. Based on these insights, the transferred impulse to the specimen had to be
4 corrected for diffraction and ground reflection.
5
6

7
8
9 These findings are very important for the correct interpretation of the efficiency of the
10 sacrificial cladding in the larger-scale blast tests (see next section), because apparent losses of
11 reflected impulse can strongly bias the conclusions about efficiency of the proposed sacrificial
12 cladding solution.
13
14
15
16
17

18 **3 Materials and methods for large-scale blast tests**

19
20
21
22
23
24
25

26 The global view of the experimental test set-up is shown in Figure 13. The glass/polyester
27 tubes were mounted on a (rear) sandwich composite skin plate behind which three dynamic
28 force sensors were connected to a concrete wall to measure the transferred impulse to the
29 concrete structure (which has to be protected from the blast). The locations of the force
30 sensors were equidistant from the centre and the angle between these sensors was 120° .
31
32
33
34
35
36
37
38
39
40
41
42
43
44
45
46
47
48
49
50
51
52
53
54
55
56
57
58
59
60
61
62
63
64
65

Another skin plate was assembled on the front side of the glass/polyester tubes (test specimens). The diameter of both front and rear sandwich skin plates was ϕ 0.96 m, in order to have a small clearance with the concrete pipe (ϕ 1.0 m) for easy assembly. The front skin panel was instrumented with three pressure sensors and two accelerometers to measure the reflected pressure and the acceleration of the skin plate respectively (Figure 13). The mass of the front skin panel was approximately 7.15 kg including all sensors. The crushing face of the front sandwich skin panel was in-line with the end of the concrete tube which was close to the concrete wall. The C4 charge was placed at the other end of the concrete pipe (stand-off

1 distance was 4.2 m). Blast experiments have been conducted for two configurations of the
2 composite tubes (25 and 37 tubes) with different charge masses (100g and 150g of C4).
3
4

5
6
7 To hold the composite tubes in horizontal position on the rear skin panel during blast loading,
8 soft foam holders were adhesively bonded on the rear skin panel (Figure 14(a-b)). The
9 stiffness of this foam was very less; hence, the resistance provided by the foam during the
10 blast loading can be neglected. Two high speed cameras were used to capture the crushing
11 behaviour of the glass/polyester tubes during the blast loading. Their view was similar to
12 Figure 14b.
13
14
15
16
17
18
19
20
21
22
23

24 All the skin plates used for the large-scale blast tests were manufactured by M/s Acrosoma,
25 Belgium. The sandwich composite skin plates were made of three materials (Figure 15). The
26 outer face sheets (top and bottom) were made of bi-axially balanced glass fibre with polyester
27 resin; the core structure was made of divinycell P foam. The outer face sheets were stitched
28 together straight through the foam with aramid fibres. This prevented the delamination
29 between the face sheets and the core structure.
30
31
32
33
34
35
36
37
38
39
40

41 Before conducting blast tests on the sacrificial cladding, the minimum length of the concrete
42 sewage pipe to provide a perfectly plane shock wave should be known. Hence, coupled
43 numerical simulations have been conducted for different charge masses and with different
44 lengths of concrete sewage pipes to identify the length which was required to have a perfectly
45 plane shock wave. The commercially available code Autodyn v12.1 was used for this
46 purpose. To reduce the computation time the concrete pipes and the front skin panel were
47 modelled with a rigid material. The length of a single concrete pipe was 2.1 m. Hence, the
48 discrete length was dictated by the length of one concrete tube. The air and C4 were modelled
49
50
51
52
53
54
55
56
57
58
59
60
61
62
63
64
65

1 using the *multi-material Euler formulation*. The initiation, detonation and the expansion of C4
2 were modelled using the *Jones-Wilkins-Lee (JWL)* Equation of state (EOS). Similarly, the
3
4 volume filled inside the concrete pipes with ambient air was modelled using the ideal gas
5
6 equation of state. Different lengths and charge masses have been considered to achieve a
7
8 perfectly plane shock wave at the other end of the concrete pipe. A fixed boundary condition
9
10 was used for the skin panel to calculate the reflected pressure time histories. As an example,
11
12 the simulated propagation of the pressure wave inside the concrete sewage pipes for 150g C4
13
14 with 4.2 m stand-off distance is shown in Figure 16. It can be noticed from Figure 16 that a
15
16 perfectly plane shock wave is formed at the other end of the tube.
17
18
19
20
21
22
23

24 Also, the comparison of the experimentally measured and numerically calculated (Autodyn
25
26 simulation) reflected pressure-time histories showed a very good correlation for peak reflected
27
28 pressure and the positive duration of the blast (Figure 17). It was essential to account for the
29
30 clearing of the pressure waves at the end of the concrete tube, due to the small mismatch in
31
32 diameter between the sandwich plates and the concrete pipe (ϕ 0.96 m vs. ϕ 1.0 m). Without
33
34 taking into account this clearance, the reflected impulse was overestimated by 33 % ! As
35
36 shown for the small-scale blast tests, this proves again the importance of clearing and
37
38 diffraction of the incident pressure waves.
39
40
41
42
43
44
45

46 The consolidated reflected blast parameters (peak reflected pressure, positive duration and the
47
48 corresponding reflected impulse) from the Autodyn simulations for the case of 150 g C4 are
49
50 presented in Table 1.
51
52
53
54
55

56 All pultruded small-scale composite tubes used for the large-scale blast testing were
57
58 reinforced with 18 streams of 4800 tex glass roving (P192 type from M/s OCV). The volume
59
60
61
62
63
64
65

1 fraction of the fibre was approximately 50%. The POLYLITE[®] 413-010 resin (un-accelerated,
2 non-thixotropic, medium reactive orthophthalic polyester resin) was used to manufacture the
3 composite tubes. In order to achieve a uniform and progressive deformation pattern the
4 thickness/diameter ratio of 0.045 was chosen. The dimensional and material details of the
5 composite tubes are given in Table 2. The composite tubes have been cut for 100 mm length
6 and filled with low-density foam, to achieve stable crushing with this very low wall thickness
7 of 1 mm. To induce the failure at lower crushing force, the 45° chamfering (triggering
8 mechanism) was introduced at one end of the composite tubes. Preliminary quasi-static and
9 impact investigations have been performed to check the progressive crushing deformation
10 patterns of these tubes (Figure 18).
11
12
13
14
15
16
17
18
19
20
21
22
23
24
25
26
27
28

29 **4. Experimental results**

30
31
32
33
34 The global deformation patterns of the composite tubes with 150 g of C4 are shown in Figure
35 19(a) and (b) for configuration 1 (25 tubes) and 2 (37 tubes) respectively. As an example, the
36 final deformation patterns after the blast experiment of two composite tubes for each
37 configuration are shown in Figure 20(a-d). It can be noticed from these figures that the
38 deformation patterns of the composite tubes are consistent; and all typical failure modes are
39 clearly evident (axial cracking, fibre failure, delamination, bending of petals). The average
40 deformation length for configuration 1 (25 tubes) was higher (55.7 mm) than for
41 configuration 2 (37 tubes) (33.7 mm).
42
43
44
45
46
47
48
49
50
51
52
53
54
55

56 Similar to the quasi-static and impact tests, the presence of the polyurethane foam prevented
57 the axial splitting of the tube wall. In addition to that, the low density of the polyurethane
58
59
60
61
62
63
64
65

1 foam did not affect the continuous delamination and subsequent fibre fracturing failure modes
2 which are very good irreversible energy dissipation mechanisms.
3
4
5
6

7 The experimentally measured load time histories for three different cases are shown in Figure
8 21(a-c) for 100 g of C4 with 25 composite tubes, 150 g of C4 with 25 composite tubes and
9 150 g of C4 with 37 composite tubes respectively.
10
11
12
13
14
15

16 The corresponding consolidated average parameters for these cases are given in Table 3.
17

18 The reference test (last row in Table 3) has been considered as the one, where the front skin
19 panel and the rear skin panel are placed side by side, without any tubes in between. Of course,
20 this configuration with the two sandwich panels will also absorb energy, but the effect of the
21 tubes can be isolated in this way.
22
23
24
25
26
27
28
29
30
31
32
33

34 For the case with 100 g of C4, the data from one test could not be measured due to some
35 problems. Hence, for this case the data from only one test is presented. From Figure 21(a-c)
36 and Table 3, it can be noticed that irrespective of the charge mass the peak crush load for
37 configuration 1 (25 composite tubes) remained the same. The peak crush loads for 100 g of
38 C4 and 150 g of C4 were 87.75 kN (from one test) and 86 kN (from two tests) respectively.
39 For configuration 2, the average peak crush load of 103.1 kN was noticed due to a higher
40 number of composite tubes. Similarly, the positive duration was extended approximately to
41 8.2 ms, 9.5 ms and 9.2 ms for 100 g C4 with 25 composite tubes, 150 g C4 with 25 composite
42 tubes and 150 g C4 with 37 composite tubes respectively.
43
44
45
46
47
48
49
50
51
52
53
54
55
56
57
58
59
60
61
62
63
64
65

1
2
3
4
5
6
7
8
9
10
11
12
13
14
15
16
17
18
19
20
21
22
23
24
25
26
27
28
29
30
31
32
33
34
35
36
37
38
39
40
41
42
43
44
45
46
47
48
49
50
51
52
53
54
55
56
57
58
59
60
61
62
63
64
65

There was a clear difference observed between the reflected impulse and the transferred impulse. The configuration 1 with 100 g and 150 g of C4 showed higher transferred impulses than for configuration 2 with 150 g of C4. The reason was that the lower number of composite tubes (for configuration 1) provided a lower resistance to the front skin panel and as a consequence a corresponding lower reaction load to the rear skin panel. However, for the case with 37 composite tubes (configuration 2) the reaction load to the rear skin panel was larger due to the larger number of composite tubes. Due to the larger reaction load and an inadequate bending stiffness, the rear skin panel was subjected to global bending during the initial stages of crushing. The bending of the rear skin panel (pin-supported on the three load cell sensors) was so high that its edge touched the concrete wall. Therefore, a significant load was directly transferred to the concrete wall and bypassed the load cell sensors. Therefore, the transferred impulse (integrated load time histories) measured from the load cells was lower for configuration 2 compared to configuration 1.

34
35
36
37
38
39
40
41
42
43
44
45
46
47
48
49
50
51
52

This is clearly illustrated by the sequence of high speed images in Figure 22. The edge of the shock tube is at the left, the concrete wall is at the right. The first image shows the "flash" when the C4 explosive detonates at the other side of the shock tube. In the second picture, the clearing of the pressure waves through the radial gap between the inner diameter of the shock tube and the front skin panel can be seen clearly. The third picture shows the progressive crushing. The fourth picture shows the severe bending of the front and rear skin panel in the top of the picture. The fifth picture shows the negative phase of the blast, where the front skin panel is "sucked" back into the shock tube.

53
54
55
56
57
58
59
60
61
62
63
64
65

The duration of the negative phase in all experiments appeared to be very long. In almost all experiments, the front skin plate could be found back at the entrance of the shock tube after the test. The large underpressure made the front skin panel travel backwards through the

1 complete length of the 4.2 m long shock tube. At the same time, it confirmed the very uniform
2 progressive crushing of the array of composite tubes, because the radial clearance was very
3 small (20 mm), and yet, the front skin panel moved backwards concentrically into the shock
4 tube.
5
6
7
8
9

10
11 Finally, in order to validate the observed bending behaviour of the skin panels, a numerical
12 model was built. The authors developed detailed finite element models in the past for crushing
13 of circular and square tubes [25,26], but those are computationally too expensive to apply to a
14 set of 25 or 37 composite tubes. Therefore the composite tubes were modelled in the finite
15 element simulation as equivalent energy absorbing tubes with the correct force-displacement
16 curve, but without incorporating all the observed failure modes (delamination, fibre fracture,
17 laminae bending). On the other hand, the sandwich composite skin panels were modelled in
18 detail, in order to validate the observed behaviour.
19
20
21
22
23
24
25
26
27
28
29
30

31 The numerical modelling of the sandwich composite skin panel was done as per the assembly
32 sequence in Figure 15. The top and bottom composite skin faces were modelled with shell
33 elements. The meshed shell elements were located at the centre of the thickness of each
34 composite laminate. The strength model of the divinycell P foam was represented by means of
35 the compressive crush characteristics (refer Figure 23).
36
37
38
39
40
41
42
43
44
45

46 It was assumed that the top and bottom composite plates and divinycell P foam were tied
47 together due to the stitch with aramid fibres. This was also supported by the experimental
48 observations. Accordingly a tied connection was established at the interfaces of all these parts.
49
50
51 Similar to the experimental conditions, the dynamic load cells were modelled as rigid bodies
52 to measure the load time histories. The concrete wall was modelled as a rigid body;
53
54
55
56
57
58
59
60
61
62
63
64
65

1
2
3
4
5
6
7
8
9
10
11
12
13
14
15
16
17
18
19
20
21
22
23
24
25
26
27
28
29
30
31
32
33
34
35
36
37
38
39
40
41
42
43
44
45
46
47
48
49
50
51
52
53
54
55
56
57
58
59
60
61
62
63
64
65

concrete wall. An equivalent triangular time dependent pressure was applied to the top face of the top skin panel.

The initial time increments showed that the front skin panel underwent a significant compression. Due to the applied blast pressure on the front face of the front skin panel the foam core reached its densification regime and it stayed in that regime until the test specimens reached their maximum deformation length. There was no significant compression observed in the rear skin panel until the foam core of the front skin panel reached its densification regime. The compression of the foam core of the rear skin panel started when the front skin panel reached its densification regime. However, the compression of the foam core was rather uniform through the entire surface of both front and rear skin panel. When the composite tubes reached their maximum deformation length, the entire rear skin panel started to bend. Subsequently, the rear skin panel came into contact with the concrete wall. A similar evidence was also noticed from the experimental results. Furthermore, a local compression of the skin plates (both front and rear) was significant at the individual mounting locations of the composite tubes, where the local reaction forces were transferred to the skin plate.

As an example, the fibre and matrix failure modes of the bottom face of the rear skin panel and bottom face of the front skin panel are shown in Figure 24(a-d) and Figure 25(a-b). It can be noticed that the tensile failure of fibres and matrix was significant. The shell elements at the load cell mounting locations showed a complete failure. The same evidence was observed from the experimental results; the foam core at the mounting locations delaminated from the face plates. Similarly, for the front skin panel, high chances of failure can be expected for the areas which were in contact with the composite tubes. Finally, the stress distribution of the foam core (divinycell P foam) of the rear skin panel is shown in Figure 26.

5 Conclusions

The small-scale blast tests on pultruded composite tubes lead to the following conclusions:

- in addition to several parameters such as the thickness/diameter ratio, linear density and triggering mechanisms, the uniform distribution of the wall thickness plays a significant role to achieve progressive deformation patterns in thin-walled composite tubes. For the chosen composite tubes (pultruded glass polyester composite tubes with wall thickness of 1.0 mm) the catastrophic failure modes were avoided by filling the tubes with a low-density polyurethane foam.
- the conducted axial quasi-static, impact and blast experiments have shown that the deformation patterns of these composite tubes remain the same. The typical brittle failure modes such as delamination, axial cracks, lamina bending and fibre fracturing were clearly evident.
- the pultruded composite tubes showed no sensitivity for strain rate, in the complete range of quasi-static to blast loading. This is due to the unidirectional fibre reinforcement.

Further, larger-scale blast tests have been conducted to understand the blast mitigation performance of a sacrificial cladding with an array of composite tubes. Tests have been conducted on two configurations of the composite tubes (25 and 37) with two charge masses of C4 (100 g and 150 g). From the conducted experimental tests the following conclusions can be made.

- The adopted concept of using two segments of concrete sewage pipes (4.2 m in length) provided a perfectly plane shock wave at the other end of the tube (crushing end). Furthermore, the negative phase of the blast load played a major role. It was observed

1 that the front skin panel was pulled back into the pipe during the negative phase.

2 Hence, proper precautions should be taken to prevent the breakage of data measuring
3 sensors and their wiring harness.
4

- 5
6
7 • The coupled numerical simulations using Autodyn predicted very close results
8 compared to the experimental results. The peak reflected pressure, positive duration
9 and the corresponding reflected impulse from the coupled numerical simulations were
10 very close to the experimental results. The radial clearance between the front skin
11 panel and the inner surface of the concrete pipe played a significant role for the total
12 reflected impulse. Due to the clearing of the reflected pressure wave (through the
13 radial clearance) the total reflected impulse was reduced. Hence, to predict accurate
14 blast parameters the same experimental boundary conditions have to be used in the
15 numerical model.
16
17 • The average peak crush load of the configuration 1 and 2 (25 and 37 composite tubes
18 respectively) was 86.5 kN and 103.1 kN respectively. Progressive crushing was
19 achieved for all tests and the transferred loads were reduced compared to the reference
20 case.
21
22 • Local bending of the front skin panel and global bending of the rear skin panel were
23 noticed. Due to that, the rear skin panel came into direct contact with the concrete wall
24 for a longer time. As a result, a significant part of the load was directly transferred to
25 the concrete wall. Therefore, there was a difference in the reflected impulse and the
26 transferred impulse noticed. Hence, for future tests the rear skin panel (sandwich
27 composite panel) should be replaced with an alternative material/structure with an
28 adequate bending stiffness. However the weight of the skin panels should be very low
29 to minimize the inertia effects.
30
31
32
33
34
35
36
37
38
39
40
41
42
43
44
45
46
47
48
49
50
51
52
53
54
55
56
57
58
59
60
61
62
63
64
65

Acknowledgements

The authors gratefully acknowledge the financial support of the “Fund for Scientific Research” – Flanders (F.W.O) (Grant No: G.0114.07).

References

- [1] S. Guruprasad and Abhijit Mukherjee, Layered sacrificial claddings under blast loading Part I -- analytical studies. *International Journal of Impact Engineering*, 2000. 24(9): p. 957-973.
- [2] S. Guruprasad and Abhijit Mukherjee, Layered sacrificial claddings under blast loading Part II -- experimental studies. *International Journal of Impact Engineering*, 2000. 24(9): p. 975-984.
- [3] C.Derdas and V.Kostopoulos C.Kotzialis, Blast behaviour of plates with sacrificial cladding. 5th GRACM International congress on computational mechanics, 2005.
- [4] A. G. Hanssen, L. Enstock and M. Langseth, Close-range blast loading of aluminium foam panels. *International Journal of Impact Engineering*, 2002. 27(6): p. 593-618.
- [5] C. Kotzialis, C. Derdas and V. Kostopoulos, Blast behaviour of plates with sacrificial cladding. 5th GRACM International congress on computational mechanics, June 29 - July 1, Limassol, Cyprus., 2005.
- [6] M. D. Theobald and G. N. Nurick, Experimental and numerical analysis of tube-core claddings under blast loads. *International Journal of Impact Engineering*. 37(3): p. 333-348.
- [7] Starr, C.M. and Krauthammer, T. (2005). Cladding-structure interaction under impact loads. *Journal of Structural Engineering – ASCE*, 131(8), 1178-1185.
- [8] A. G. Mamalis, D. E. Manolakos and G. A. Demosthenous, *Crushing behaviour of thin-walled, non-circular, glass fibre-reinforced composite tubular components due to bending*. *Composites*, 1992. 23(6): p. 425-433.
- [9] A. G. Mamalis, D. E. Manolakos, G. A. Demosthenous and M. B. Ioannidis, *Energy absorption capability of fibreglass composite square frusta subjected to static and dynamic axial collapse*. *Thin-Walled Structures*, 1996. 25(4): p. 269-295.
- [10] A. G. Mamalis, D. E. Manolakos, M. B. Ioannidis and D. P. Papapostolou, *Crashworthy characteristics of axially statically compressed thin-walled square CFRP composite tubes: experimental*. *Composite Structures*, 2004. 63(3-4): p. 347-360.
- [11] A. G. Mamalis, M. Robinson, D. E. Manolakos, G. A. Demosthenous, M. B. Ioannidis and J. Carruthers, *Crashworthy capability of composite material structures*. *Composite Structures*, 1997. 37(2): p. 109-134.
- [12] S. Solaimurugan and R. Velmurugan, *Progressive crushing of stitched glass/polyester composite cylindrical shells*. *Composites Science and Technology*, 2007. 67(3-4): p. 422-437.
- [13] G L and Jones Farley, R.M, *Analogy for the effect of material and geometrical variables on energy absorption capability of composite tubes*. *Journal of Composite Materials*, 1992. 26: p. 78.
- [14] P. H. Thornton, *The crush behavior of pultruded tubes at high strain rates*. *Journal of Composite Materials*, 1989. 24: p. 22.
- [15] H. Hamada, J. C. Coppola, D. Hull, Z. Maekawa and H. Sato, *Comparison of energy absorption of carbon/epoxy and carbon/PEEK composite tubes*. *Composites*, 1992. 23(4): p. 245-252.
- [16] S. Ramakrishna and D. Hull, *Energy absorption capability of epoxy composite tubes with knitted carbon fibre fabric reinforcement*. *Composites Science and Technology*, 1993. 49(4): p. 349-356.
- [17] S. Chung Kim Yuen and G. N. Nurick, The energy absorbing characteristics of tubular structures with geometric and material modifications: an overview, *Applied Mechanics Reviews*, Volume 61 (2008). 020802 (15 pages)
- [18] D. Karagiozova, G. N. Nurick, S. Chung Kim Yuen, Energy absorption of aluminium alloy circular and square tubes under an axial explosive load, *Thin-Walled Structures*, Volume 43 (2005), 956-982.
- [19] M. D. Theobald and G. N. Nurick Numerical investigation of the response of sandwich-type panels using thin-walled tubes subject to blast loads, *International Journal of Impact Engineering*, Volume 34 (2007), 134-156.
- [20] C. J. McGregor, R. Vaziri, A. Poursartip, X. Xiao, Simulation of progressive damage development in

- braided composite tubes under axial compression, *Composites Part A: Applied Science and Manufacturing*, Volume 38 (2007), 22472259.
- [21] Palanivelu, S., Van Paepegem, W., Degrieck, J., Van Ackeren, J., Kakogiannis, D., Van Hemelrijck, D., Wastiels, J. and Vantomme, J. (2010). Experimental study on the axial crushing behaviour of pultruded composite tubes. *Polymer Testing*, 29(2), 224-234.
- [22] Palanivelu, S., Van Paepegem, W., Degrieck, J., Kakogiannis, D., Van Ackeren, J., Van Hemelrijck, D., Wastiels, J. and Vantomme, J. (2010). Comparative study of the quasi-static energy absorption of small-scale composite tubes with different geometrical shapes for use in sacrificial cladding structures. *Polymer Testing*, 29(3), 381-396.
- [23] Palanivelu, S., Van Paepegem, W., Degrieck, J., Vantomme, J., Kakogiannis, D., Van Ackeren, J., Van Hemelrijck, D. and Wastiels, J. (2010). Comparison of the crushing performance of hollow and foam-filled small-scale composite tubes with different geometrical shapes for use in sacrificial cladding structures. *Composites Part B: Engineering*, 41(6), 434-445.
- [24] Palanivelu, S., Van Paepegem, W., Degrieck, J., Vantomme, J., Kakogiannis, D., Van Ackeren, J., Van Hemelrijck, D. and Wastiels, J. (2011). Crushing and energy absorption performance of different geometrical shapes of small-scale glass/polyester composite tubes under quasi-static loading conditions. *Composite Structures*, 93(2), 992-1007.
- [25] Palanivelu, S., Van Paepegem, W., Degrieck, J., Kakogiannis, D., Van Ackeren, J., Van Hemelrijck, D., Wastiels, J. and Vantomme, J. (2010). Parametric study of crushing parameters and failure patterns of pultruded composite tubes using cohesive elements and seam. Part I –Central delamination and triggering modelling. *Polymer Testing*, 29(6), 729-741.
- [26] Palanivelu, S., Van Paepegem, W., Degrieck, J., Van Ackeren, J., Kakogiannis, D., Wastiels, J., Van Hemelrijck, D., and Vantomme, J. (2010). Parametric study of crushing parameters and failure patterns of pultruded composite tubes using cohesive elements and seam. Part II – Multiple delaminations and initial geometric imperfections. *Polymer Testing*, 29(7), 803-814.
- [27] Kakogiannis, D., Chung Kim Yuen, S., Palanivelu, S., Van Hemelrijck, D., Van Paepegem, W., Wastiels, J., Vantomme, J. and Nurick, G.N. (2013). Response of pultruded composite tubes subjected to dynamic and impulsive axial loading. *Composites Part B: Engineering*, 55, 537-547.
- [28] Thornton, P. H., The crush behavior of pultruded tubes at high strain rates. *Journal of Composite Materials*, 1989. 24: p. 22.

Table 1: Comparison of experimental measurements and calculated blast parameters from Autodyn simulations without and with a radial clearance between the front skin panel and the concrete pipe for a charge mass of 150 g C4.

Parameters	Pressure sensor 1	Pressure sensor 2	Pressure sensor 3
Experimental			
Peak reflected pressure (kPa)	561.5	525.2	530.8
Positive duration (ms)	5.2	4.9	5.1
Reflected impulse (kPa.ms)	627.1	685.3	737.6
Numerical simulation without considering the radial clearance			
Peak reflected pressure (kPa)	590		
Positive duration (ms)	6.2		
Reflected impulse (kPa.ms)	908		
Numerical simulation with considering the radial clearance			
Peak reflected pressure (kPa)	564		
Positive duration (ms)	5.24		
Reflected impulse (kPa.ms)	679		

Table 2: Dimensional and material details of the composite tube series.

Cross-section	Fibre	Resin	Dimensions (mm)	ρ_{linear} (g/mm)	Volume fraction (%)
Circular	Glass	Polyester	$\phi = 22$ $t = 1$ $L = 100$	0.14 without foam	$V_m = \sim 50$
				0.15 with foam	$V_f = \sim 50$
ϕ - Outer diameter; t - thickness; L - length of tube; V_m - volume fraction of matrix; V_f - volume fraction of fibre.					

1
2
3
4
5
6
7
8
9
10
11
12
13
14
15
16
17
18
19
20
21
22
23
24
25
26
27
28
29
30
31
32
33
34
35
36
37
38
39
40
41
42
43
44
45
46
47
48
49

Table 3: Summary of crushing parameters.

Charge mass	No. composite tubes	Stand-off distance	Load cells data	Peak crush load	Total peak crush load	Time for load transfer	Average time	Reflected impulse (from Autodyn)	Transferred impulse	Total transferred impulse	Average deformation length		
(g)		(m)		(kN)	(kN)	(ms)	(ms)	(kN.ms)	(kN.ms)	(kN.ms)	(mm)		
Test with configuration 1 (25 composite tubes)													
100	25	4.2	Load cell 1	29.5	87.7		8.2	599		85.2	249.3	25.8	
			Load cell 2	32.3						88.1			
			Load cell 3	25.9						76.0			
150	25	4.2	Load cell 1	25.4	86.6		8.4	679		87.3	267.3	33.6	
			Load cell 2	30.1						89.9			
			Load cell 3	31.1						90.1			
			Load cell 1	36.1	85.4		10.7				95.0	247.3	31.1
			Load cell 2	27.2							71.1		
			Load cell 3	22.1							81.2		
Test with configuration 2 (37 composite tubes)													
150	37	4.2	Load cell 1	30.3	104.4		9.4	679		72.5	196.1	55.2	
			Load cell 2	38.1						53.8			
			Load cell 3	36.0						69.8			
			Load cell 1	27.5	101.9		8.95				65.9	185.2	49.8
			Load cell 2	40.9							61.0		
			Load cell 3	33.5							58.3		
Reference test													
150	-	4.2	Load cell 1	48.5	138.3		4.4	679		87.9	256.6	-	
			Load cell 2	46.9						83.4			
			Load cell 3	42.9						85.3			

Figure Captions

1
2
3
4
5
6
7
8
9
10
11
12
13
14
15
16
17
18
19
20
21
22
23
24
25
26
27
28
29
30
31
32
33
34
35
36
37
38
39
40
41
42
43
44
45
46
47
48
49
50
51
52
53
54
55
56
57
58
59
60
61
62
63
64
65

Figure 1: Working principle of a sacrificial cladding structure.

Figure 2: (a) Schematic view (b) Small-scale air blast test set-up.

Figure 3: Uniform progressive crushing of the circular cross sectional glass polyester composite tubes (1 mm wall thickness) : tube 1 and 2 (30 g and 30 cm stand-off distance) and tube 3, 4 and 5 (20g and 30 cm stand-off distance).

Figure 4: Progressive deformation patterns of commercially available pultruded GFRP composite tubes (2 mm wall thickness) for free air blast loading (40g of C4) with 15 cm stand-off distance.

Figure 5: (a) Pendulum set-up for contact blast loading, (b) progressive deformation patterns of GFRP composite tubes subjected to contact blast loading condition.

Figure 6: Comparison of force-deformation curves for different loading conditions (quasi-static, impact and blast loading).

Figure 7: 2D wedge model with incident overpressure contours for 20g of C4 at 30 cm stand-off distance.

Figure 8: Comparison of incident pressure-time histories from Autodyn, ConWep and experimental measurements for 20g of C4 at 30 cm stand-off distance.

Figure 9: Coupled 3D simulation of the blast detonation and interaction with the test set-up.

Figure 10: Interaction of blast pressure waves with the aluminium skin plate.

Figure 11: Interaction of the reflected pressure wave with the skin plate from the ground surface.

Figure 12: Experimental proof of the "clearing" of the shock wave around the edges of the skin plate for 20 g TNT at 30 cm stand-off distance.

Figure 13: Schematic representation of the experimental set-up for the sacrificial cladding.

Figure 14: Large-scale blast experimental test set-up: (a) sandwich skin panel with composite tubes (25 tubes configuration) (b) Side view of assembly

Figure 15: Schematic drawing of the sandwich skin plates with glass/polyester face sheets and Divinycell P foam.

Figure 16: Autodyn simulation of the propagation of the blast pressure wave inside the concrete sewage pipes for 150 g C4.

Figure 17: Comparison of the experimentally measured and numerically calculated (reflected) pressure time histories for 150 g C4 considering a radial clearance between the front skin panel and concrete pipe.

1 Figure 18: (a) Quasi-static progressive crushing modes of composite tubes with uniform
2 thickness of 1 mm and the corresponding load-deformation curves, (b) Load-deformation
3 curves for two identical tubes under quasi-static loading.
4

5
6 Figure 19: Global deformation patterns of the composite tubes (a) configuration 1 (25
7 composite tubes) with 150 g of C4 (b) configuration 2 (37 composite tubes) with 150 g of C4.
8

9
10 Figure 20: Final deformation patterns of composite tubes (a-b) for 150 g of C4 with
11 configuration 1 (25 composite tubes). (c-d) for 150 g of C4 with configuration 2 (37
12 composite tubes)
13

14 Figure 21: Transferred load time histories (a) for 100 g of C4 with 25 tubes (b) for 150 g of
15 C4 with 25 tubes (c) for 150 g of C4 with 37 tubes.
16

17
18 Figure 22: Image sequence of crushing of 25 composite tubes (150 g C4).
19

20
21 Figure 23: Compressive crushing characteristic of the divinycell P foam.
22

23 Figure 24: Tensile and compressive failures of back face of rear skin panel (a) fibre tensile
24 failure (b) fibre compressive failure (c) matrix tensile failure (d) matrix compressive failure
25 (magnification factor 5).
26

27
28 Figure 25: Fibre and matrix failures of bottom face of the top skin panel (a) fibre tensile
29 failure (b) matrix tensile failure (magnification factor 5).
30

31 Figure 26: Stress distribution on core foam (divinycell P foam) of the rear skin panel
32 (magnification factor 5).
33
34
35
36
37
38
39
40
41
42
43
44
45
46
47
48
49
50
51
52
53
54
55
56
57
58
59
60
61
62
63
64
65

Figure 01
[Click here to download high resolution image](#)

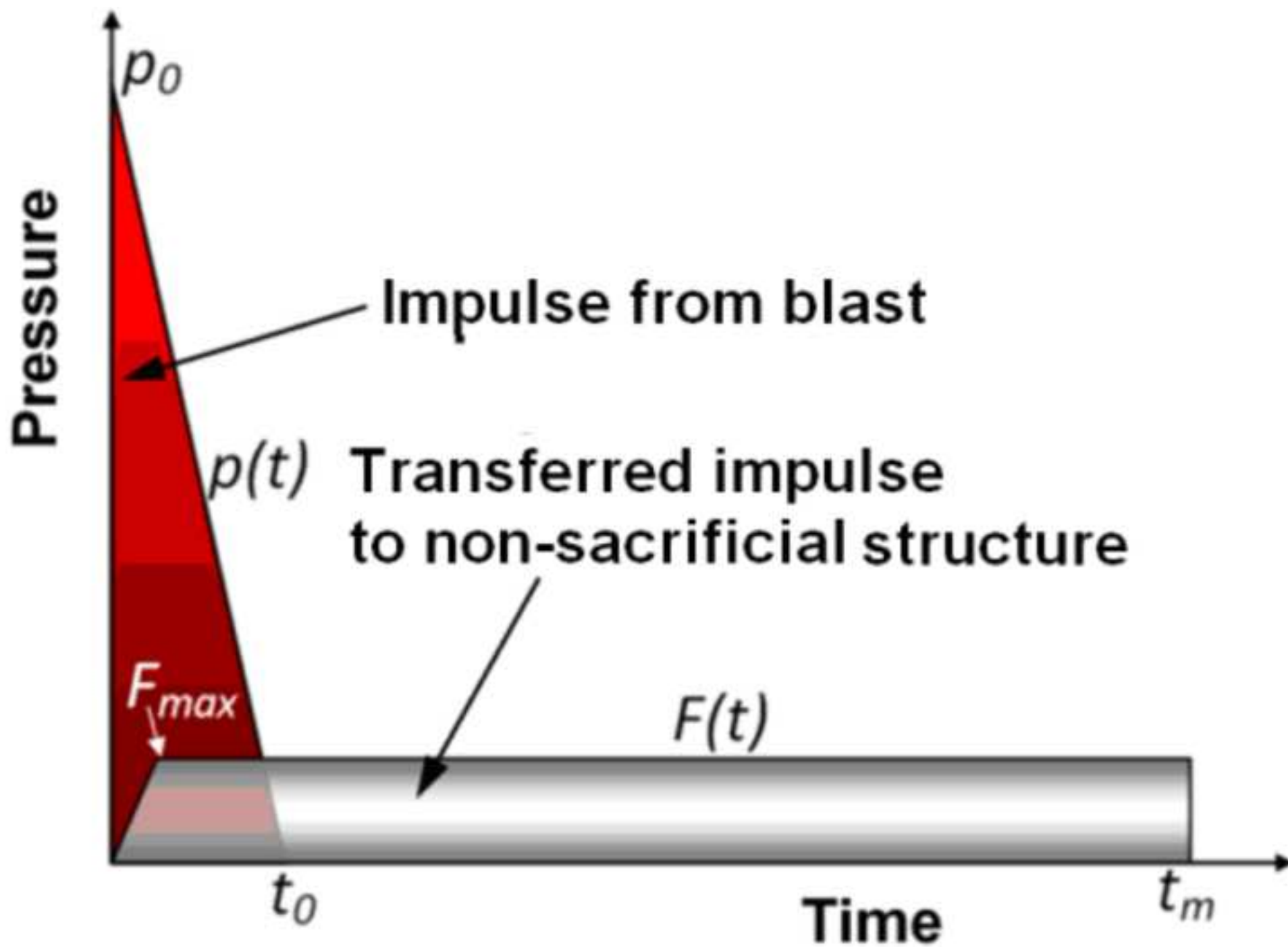


Figure 02

[Click here to download high resolution image](#)

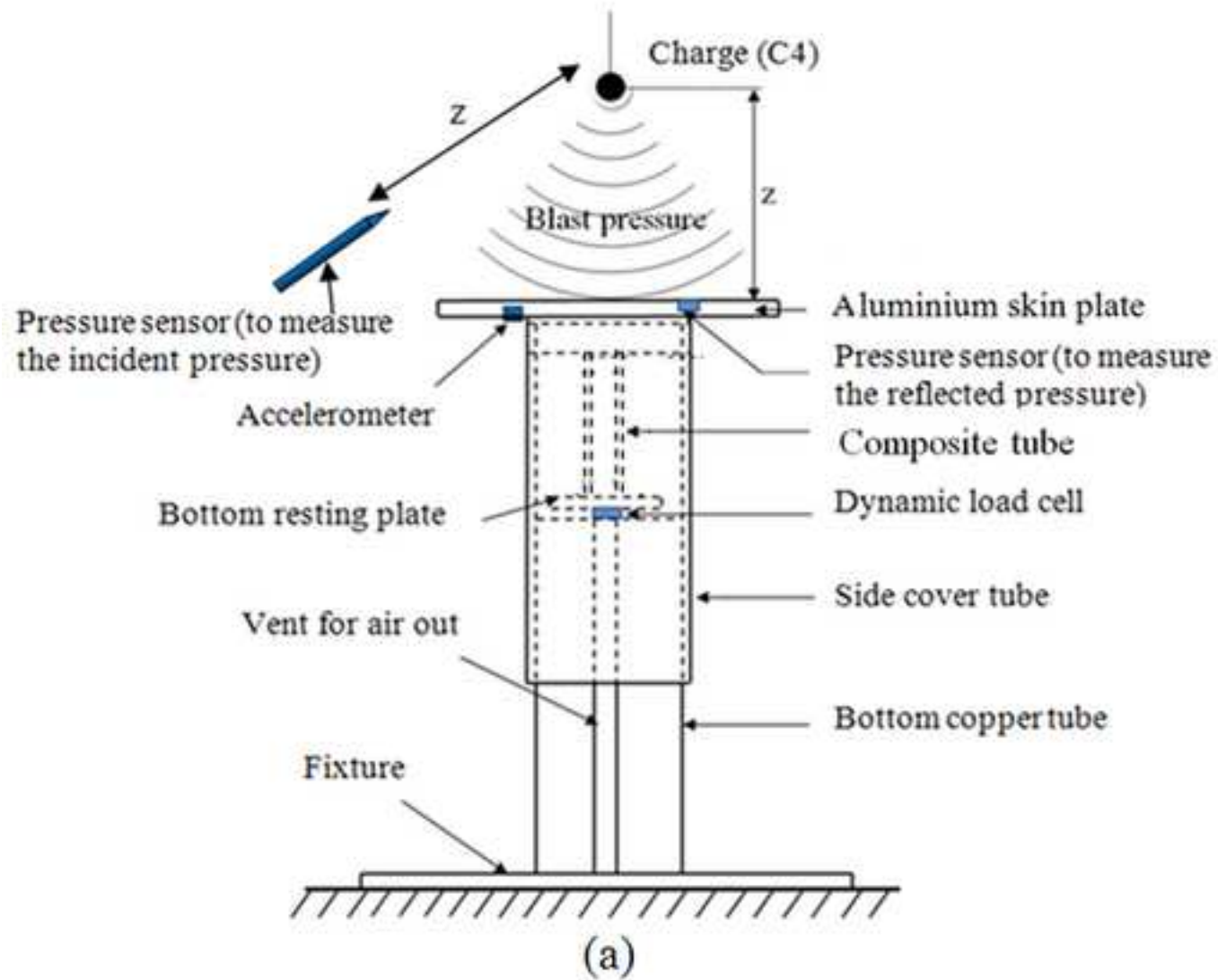


Figure 03
[Click here to download high resolution image](#)

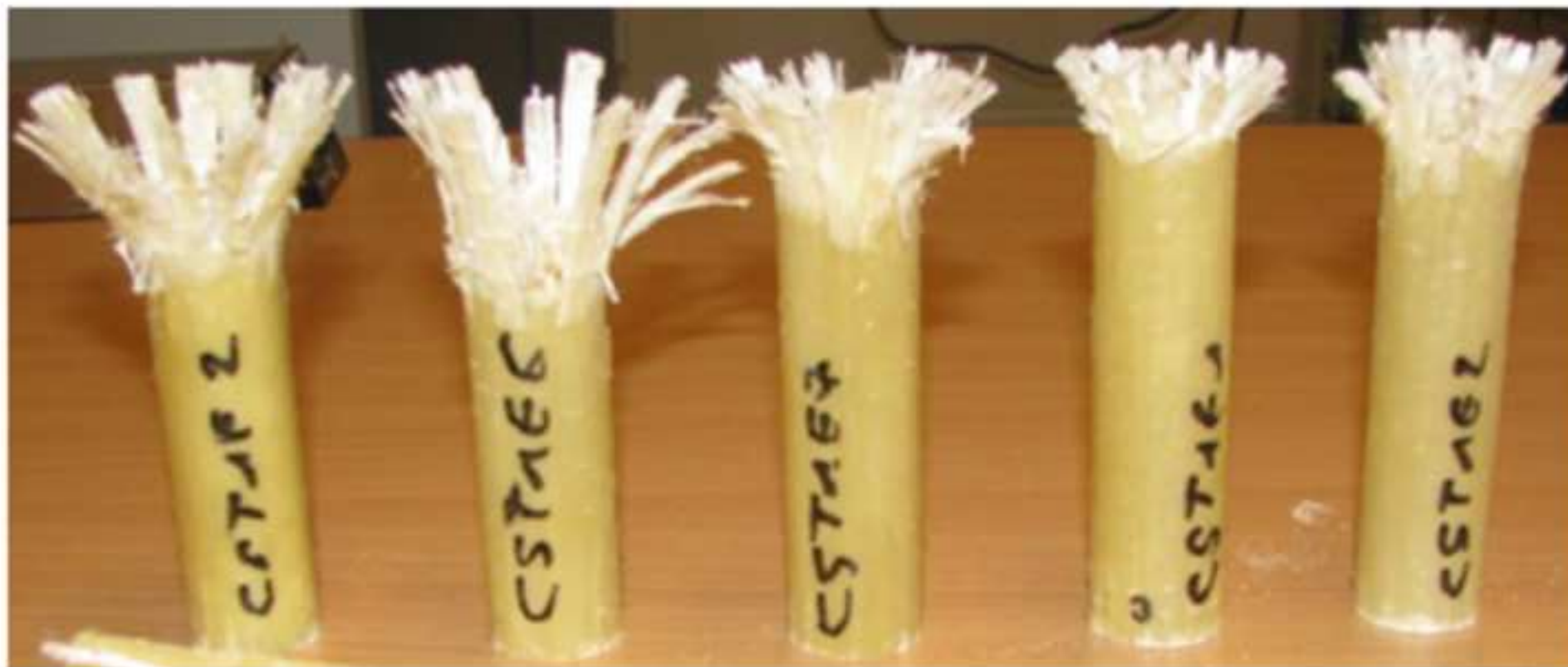


Figure 04
[Click here to download high resolution image](#)



Figure 05

[Click here to download high resolution image](#)



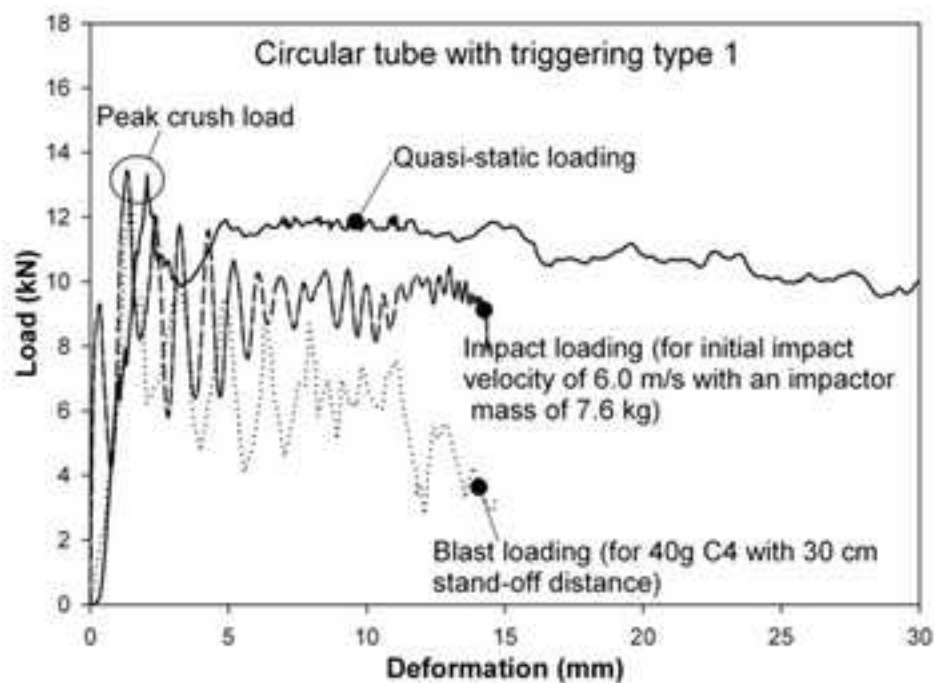
(a)



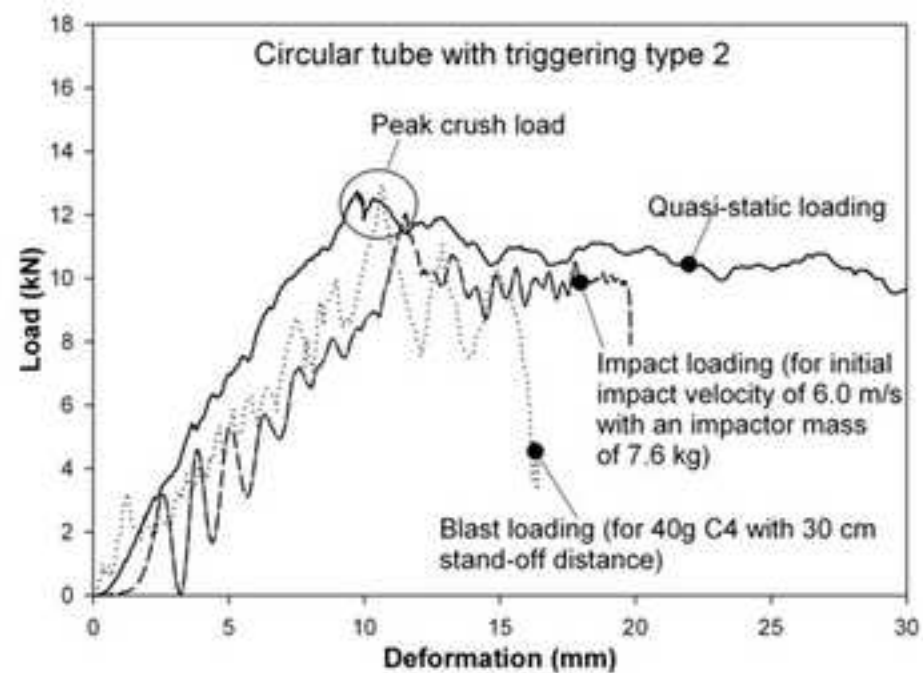
(b)

Figure 06

[Click here to download high resolution image](#)



(a) Triggering type 1



(b) Triggering type 2

Figure 07
[Click here to download high resolution image](#)

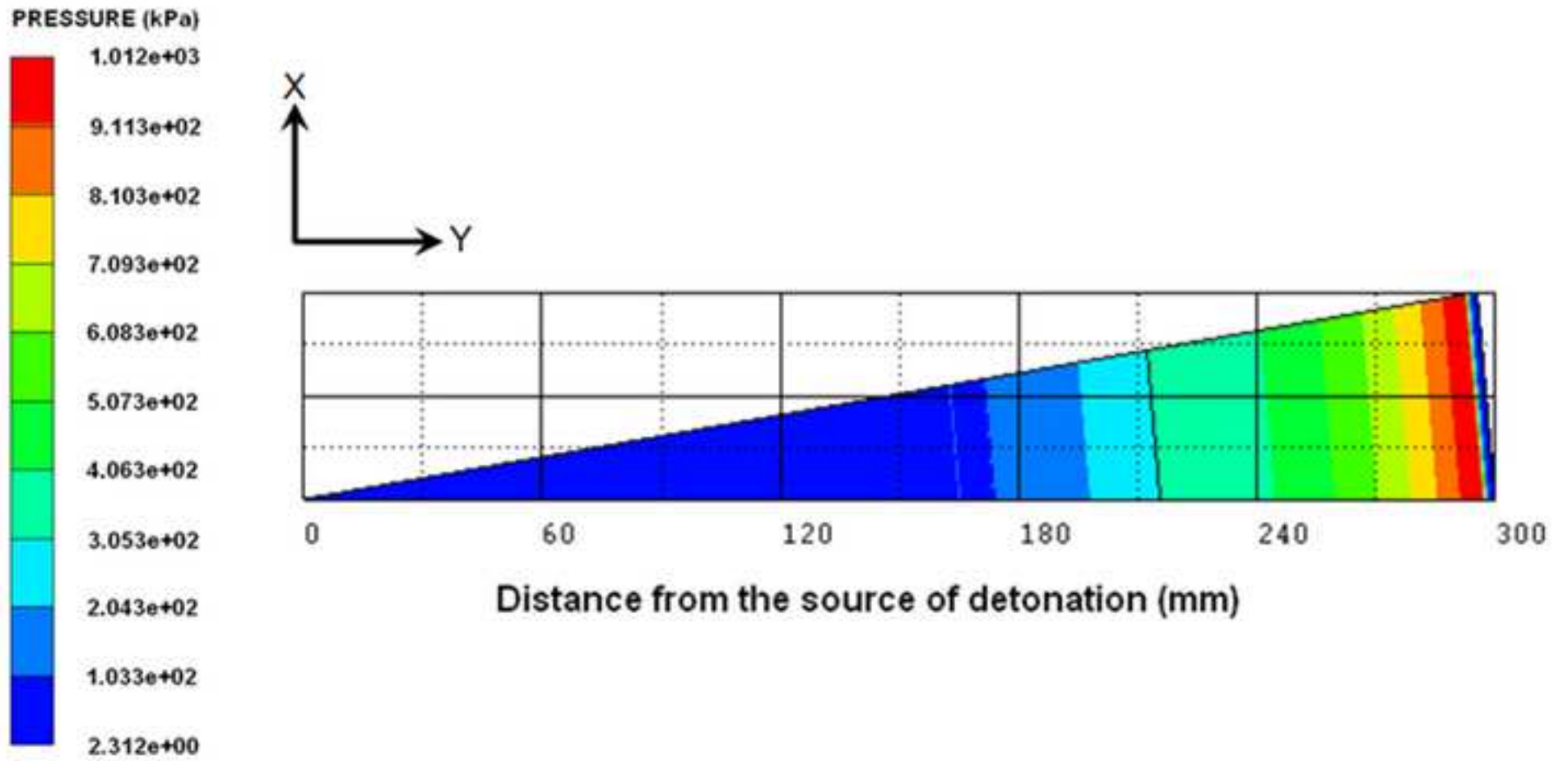


Figure 08
[Click here to download high resolution image](#)

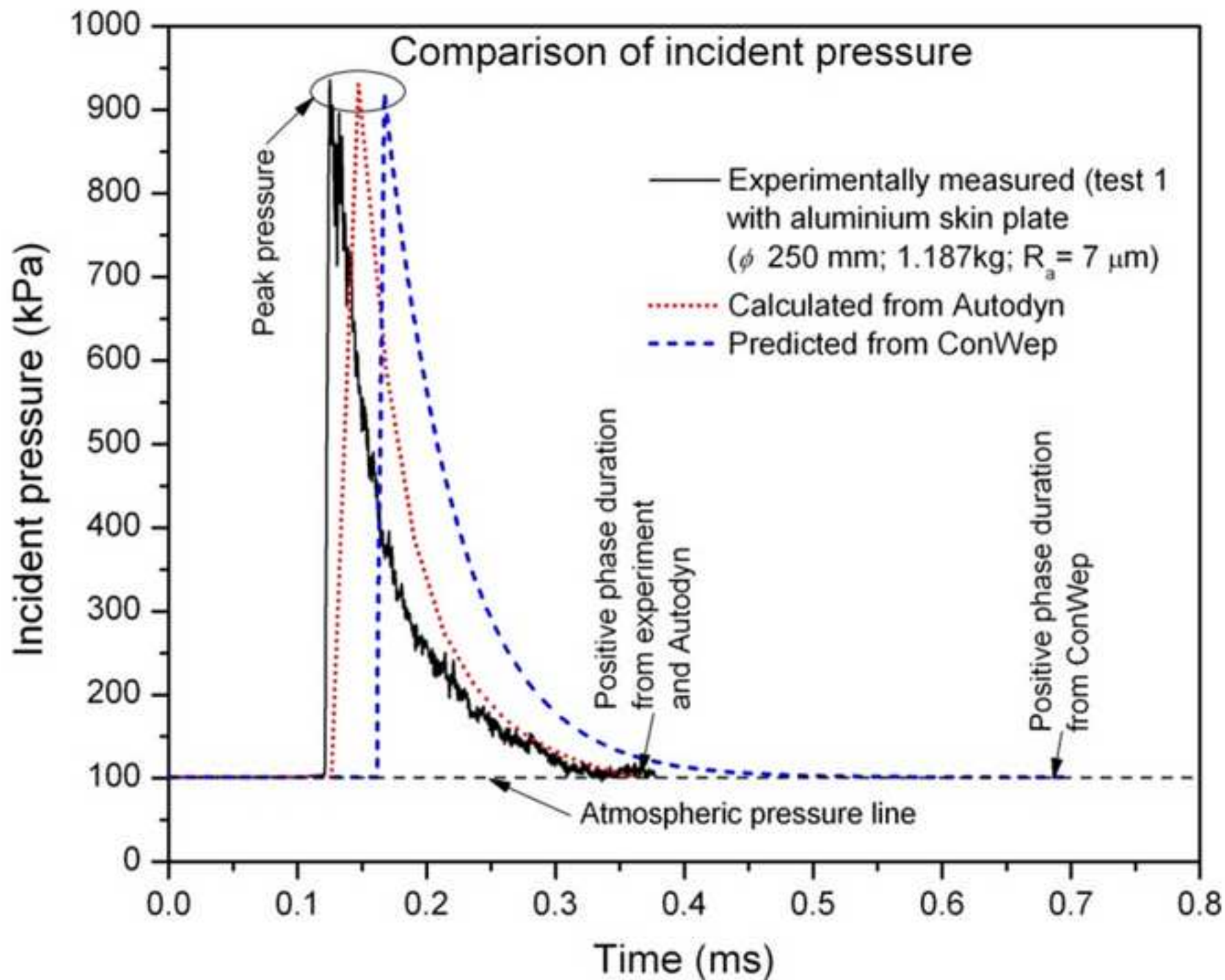


Figure 09

[Click here to download high resolution image](#)

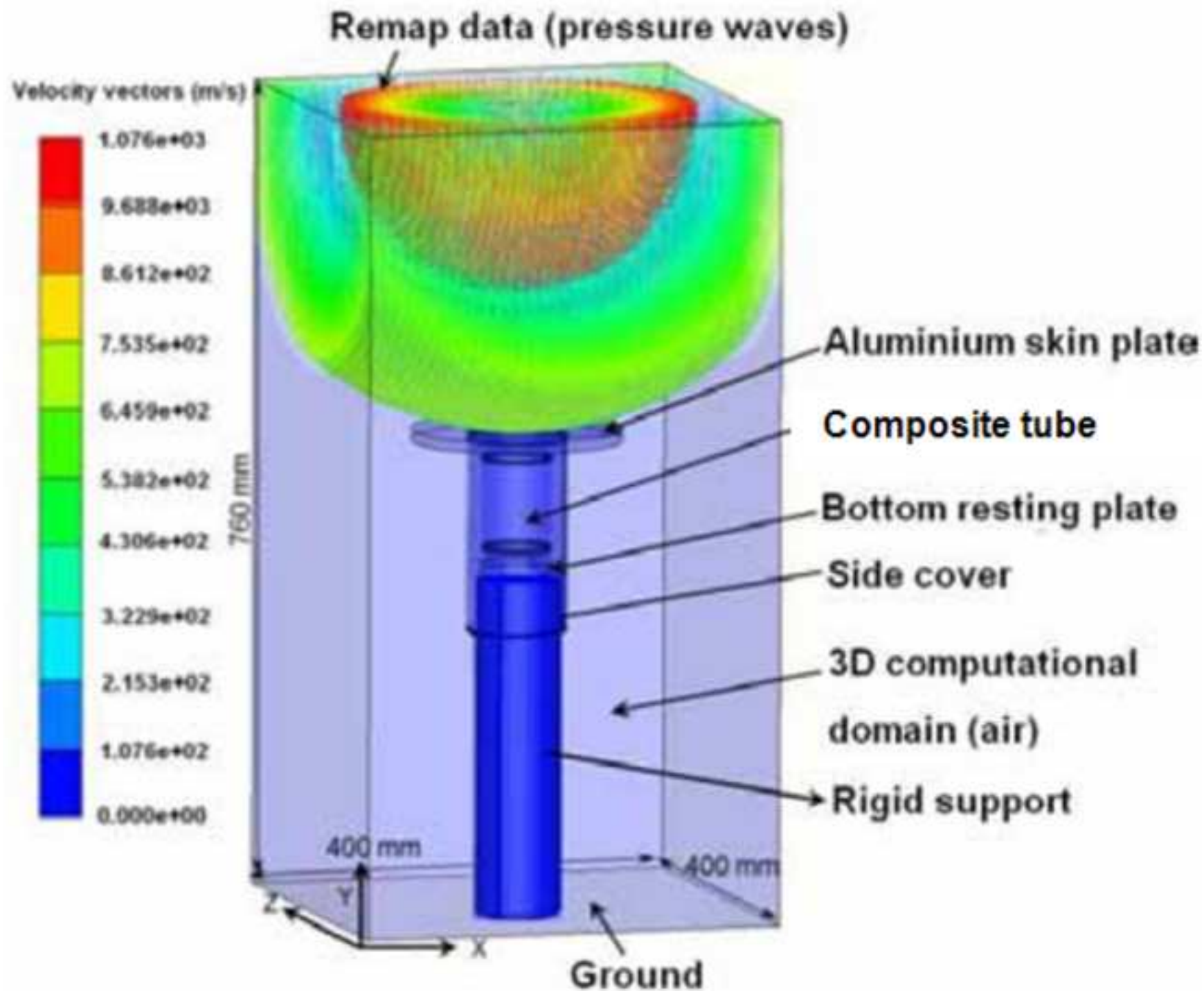


Figure 10

[Click here to download high resolution image](#)

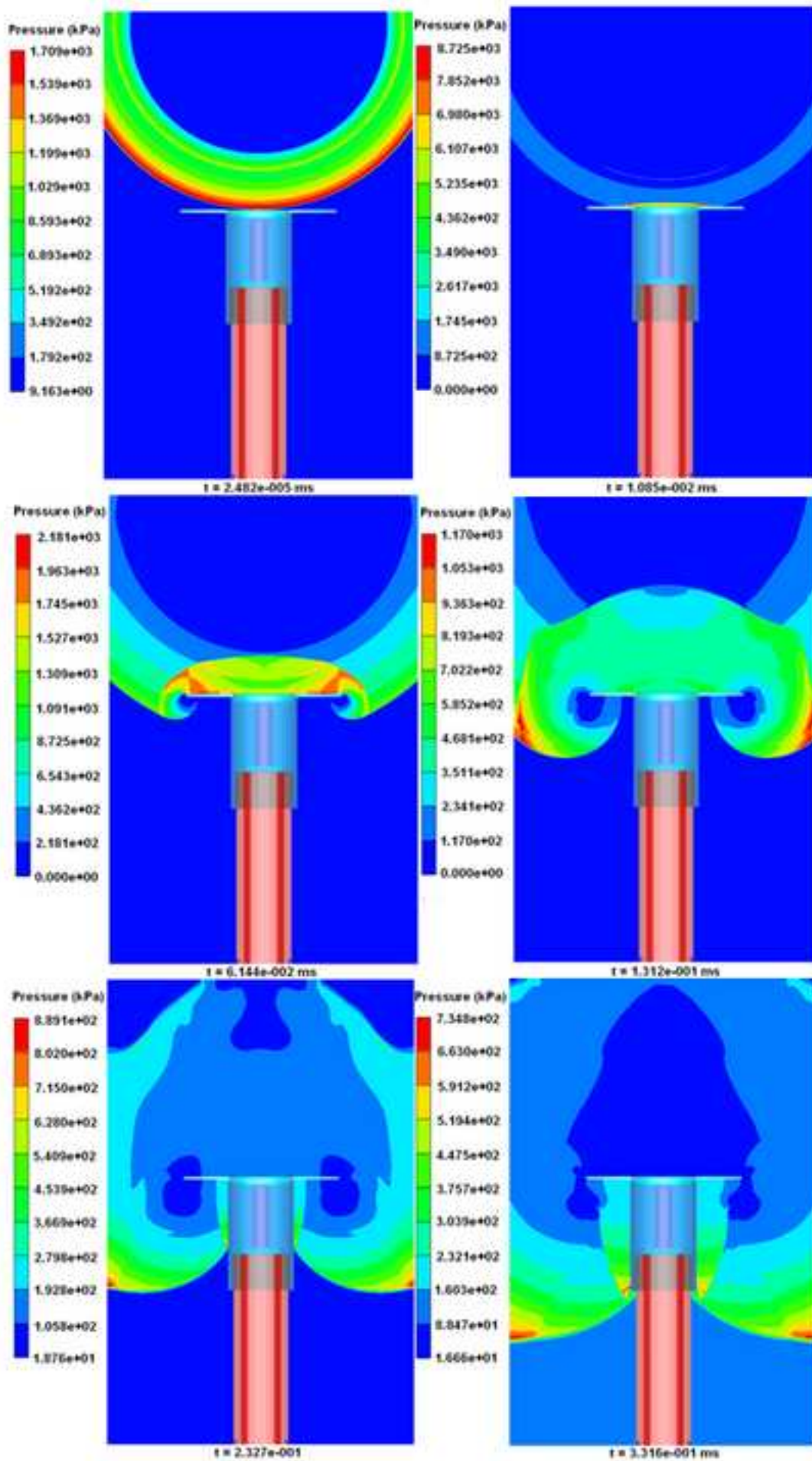


Figure 11

[Click here to download high resolution image](#)

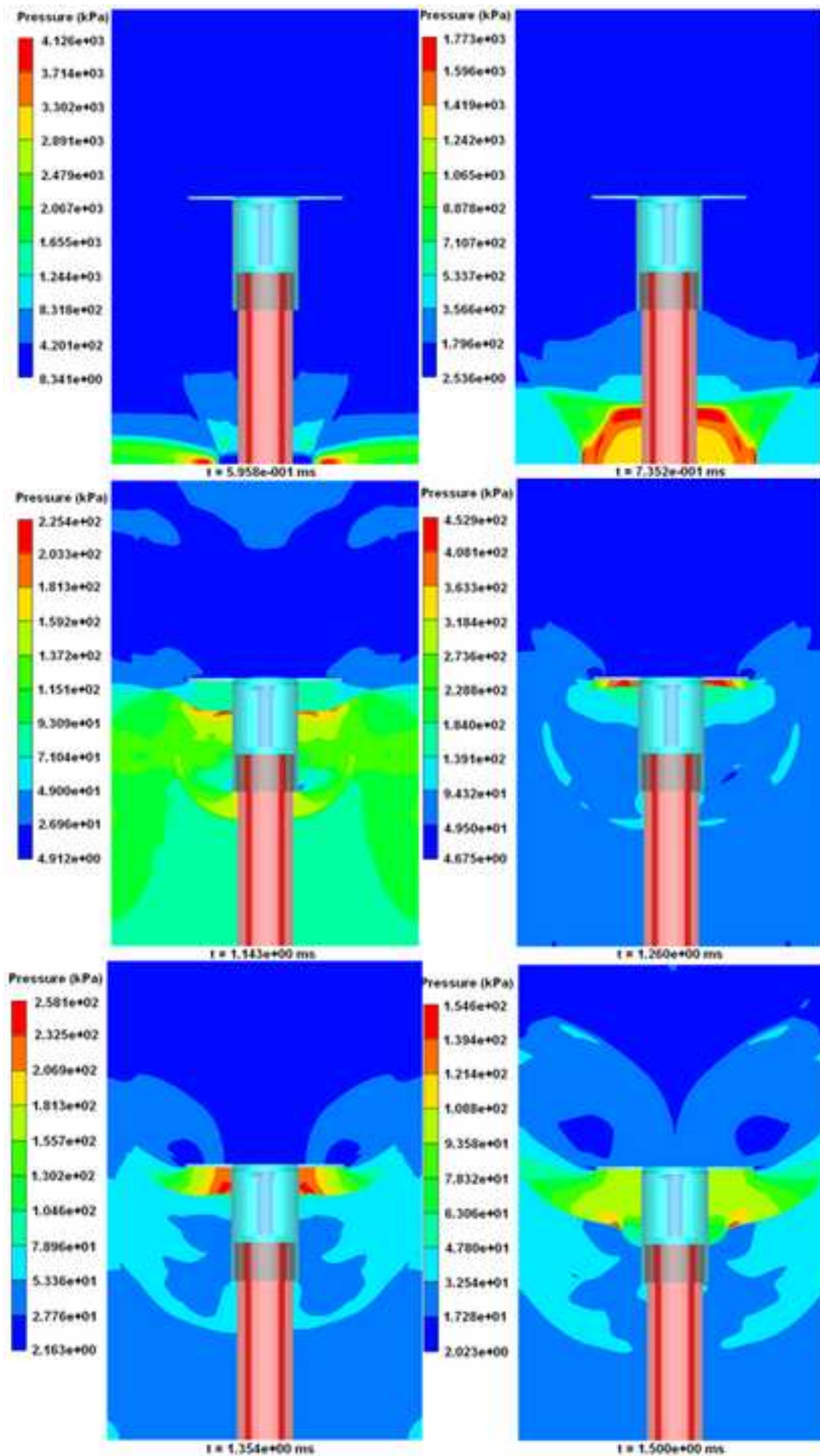


Figure 12
[Click here to download high resolution image](#)



Figure 13

[Click here to download high resolution image](#)

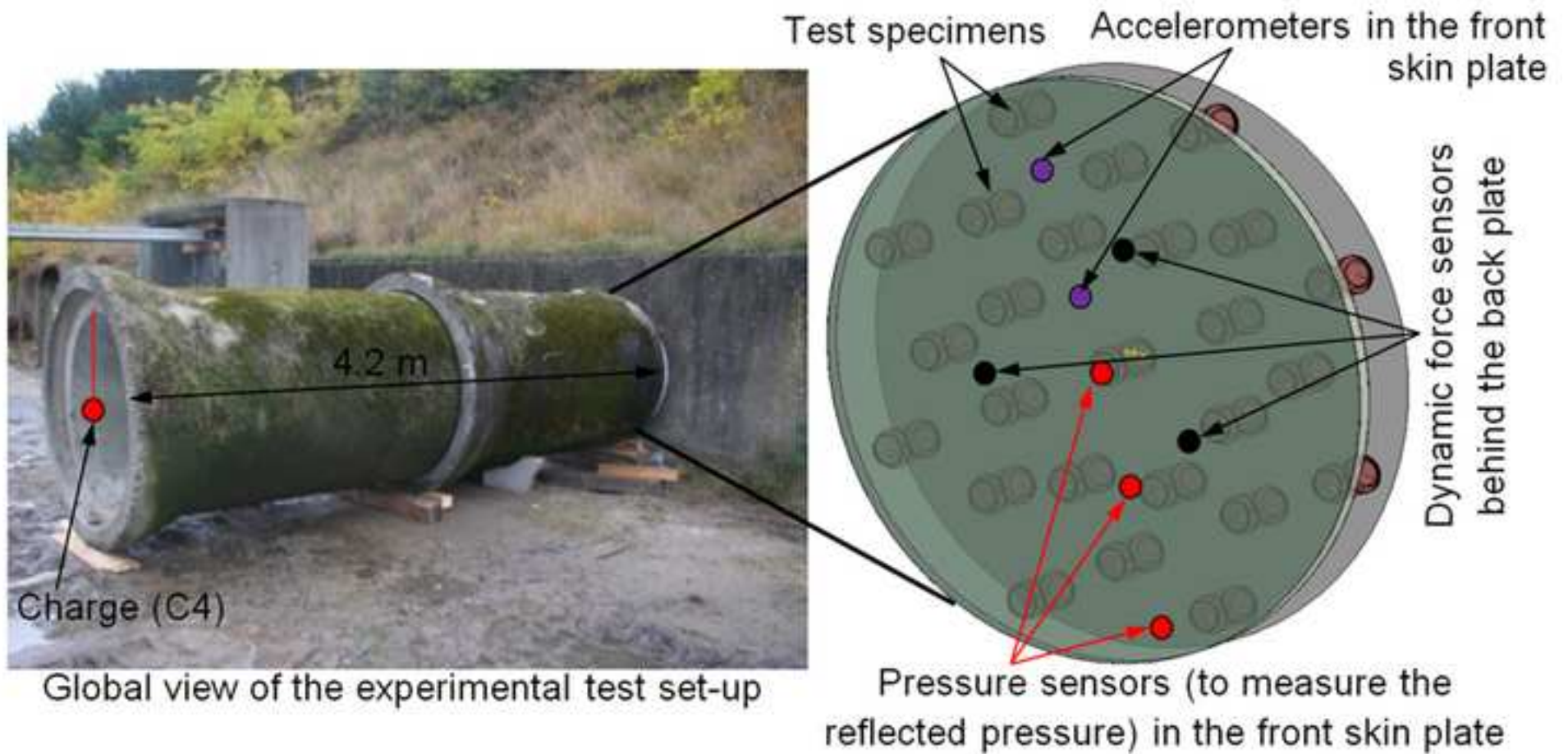


Figure 14
[Click here to download high resolution image](#)



(a)



(b)

Figure 15
[Click here to download high resolution image](#)

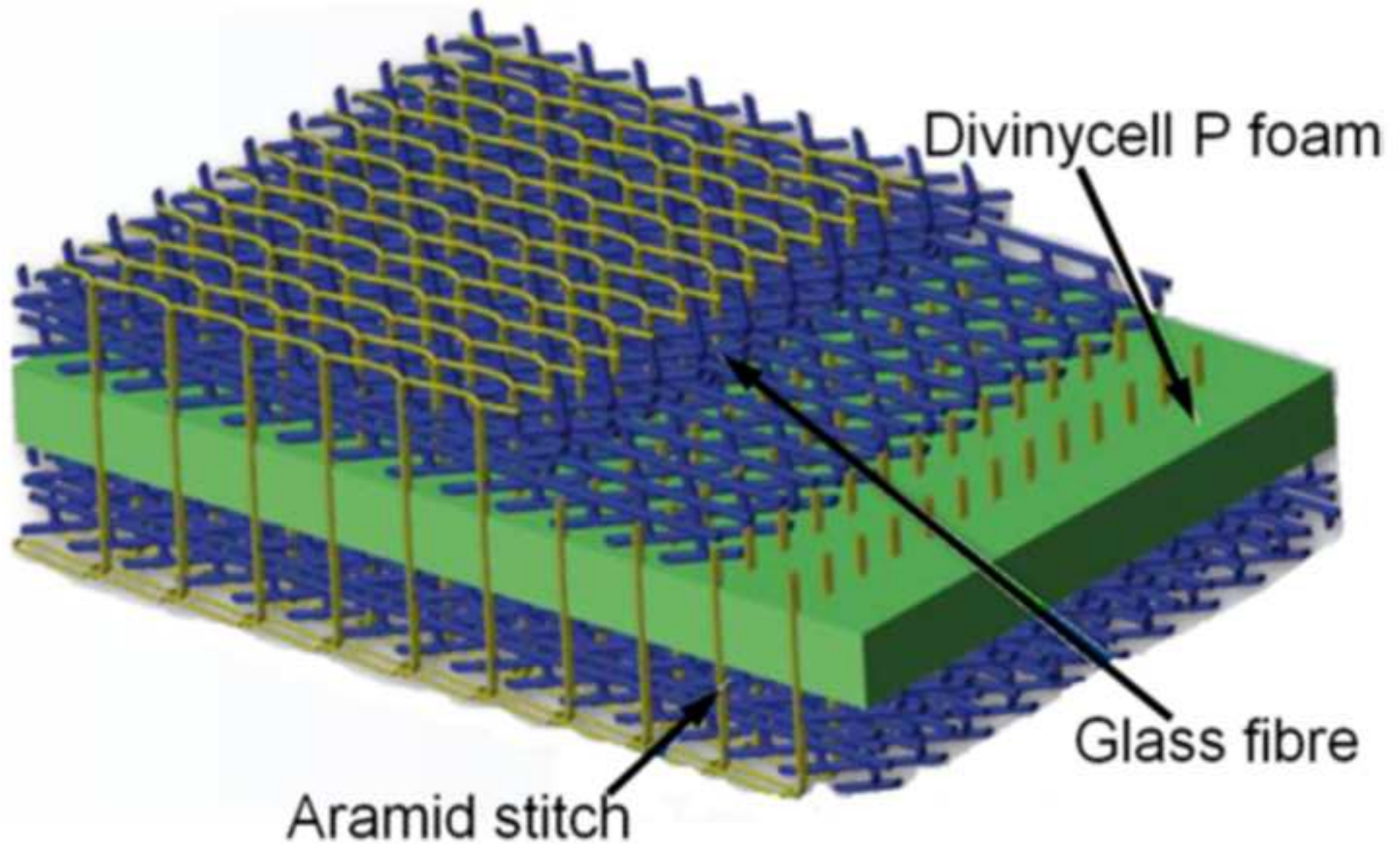


Figure 16
[Click here to download high resolution image](#)

Pressure wave Concrete sewage pipes

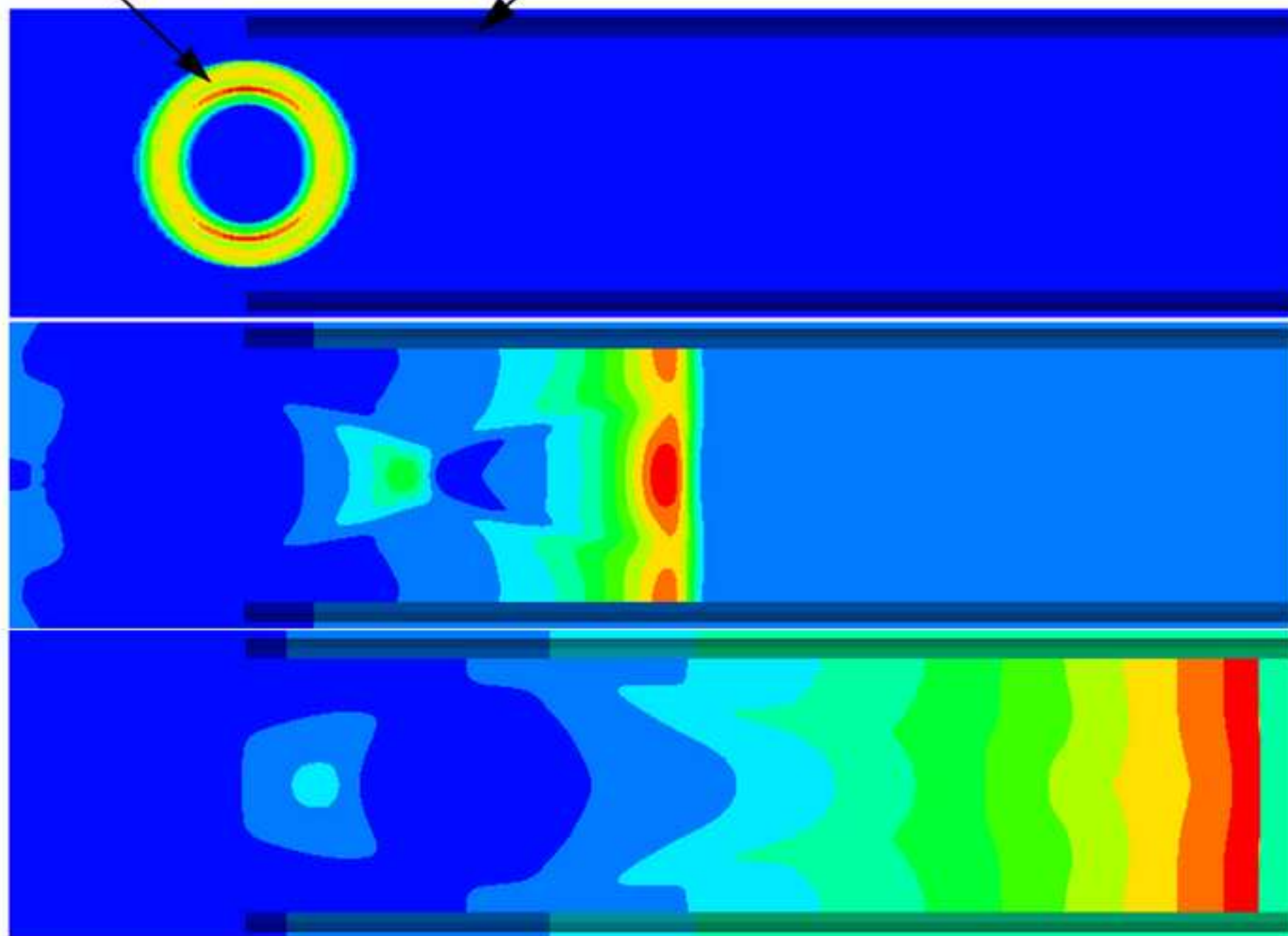


Figure 17

[Click here to download high resolution image](#)

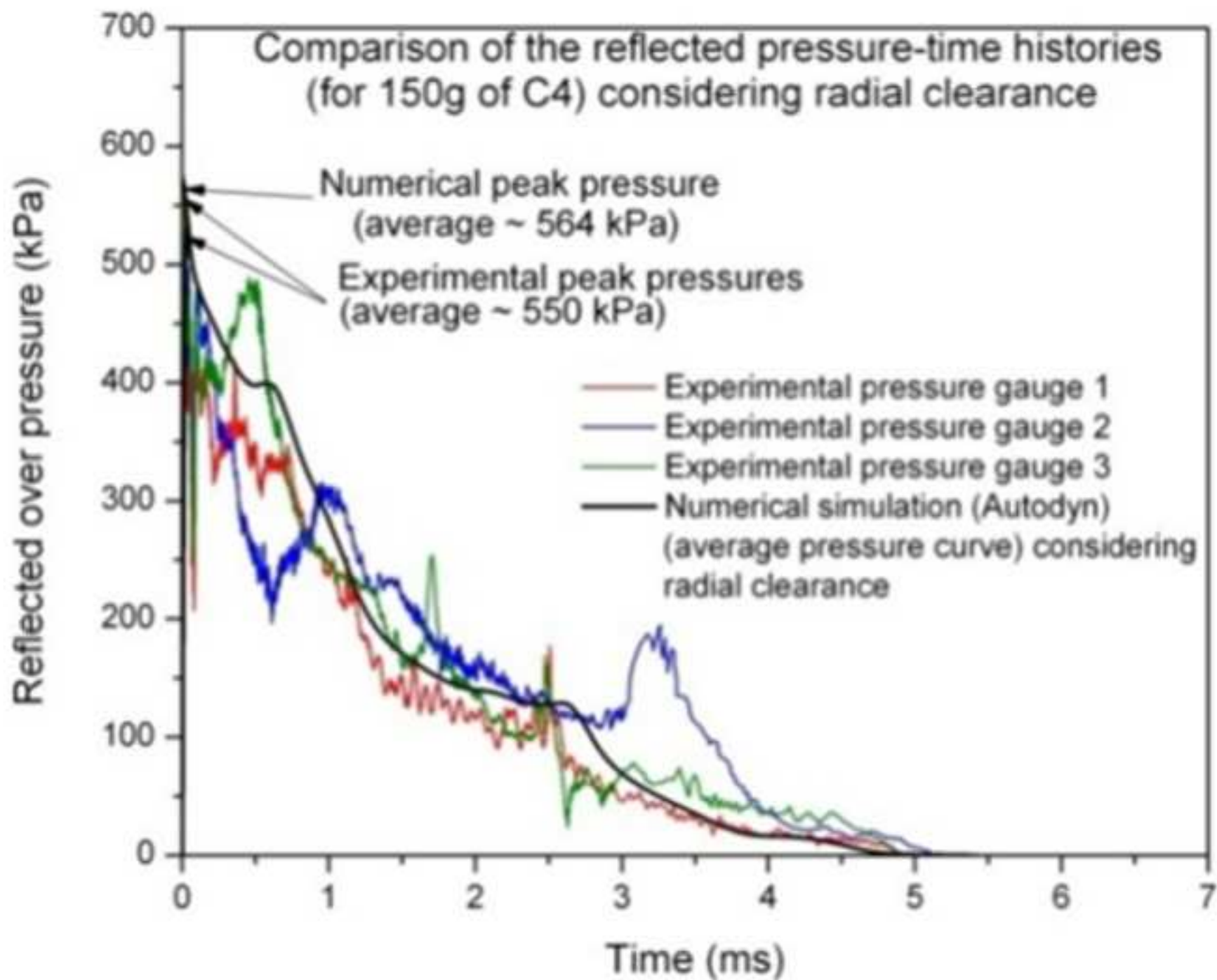
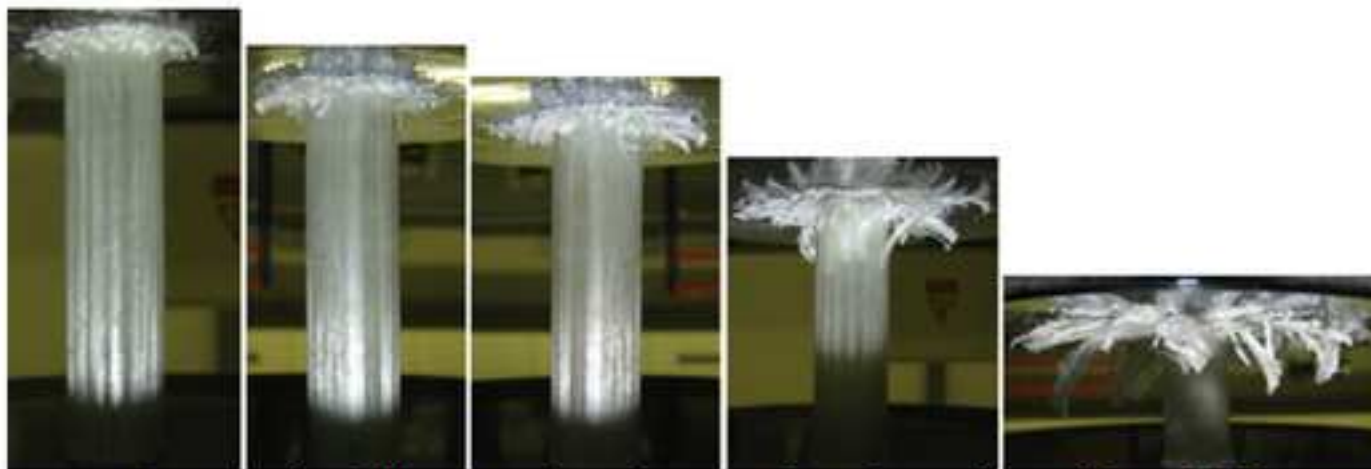
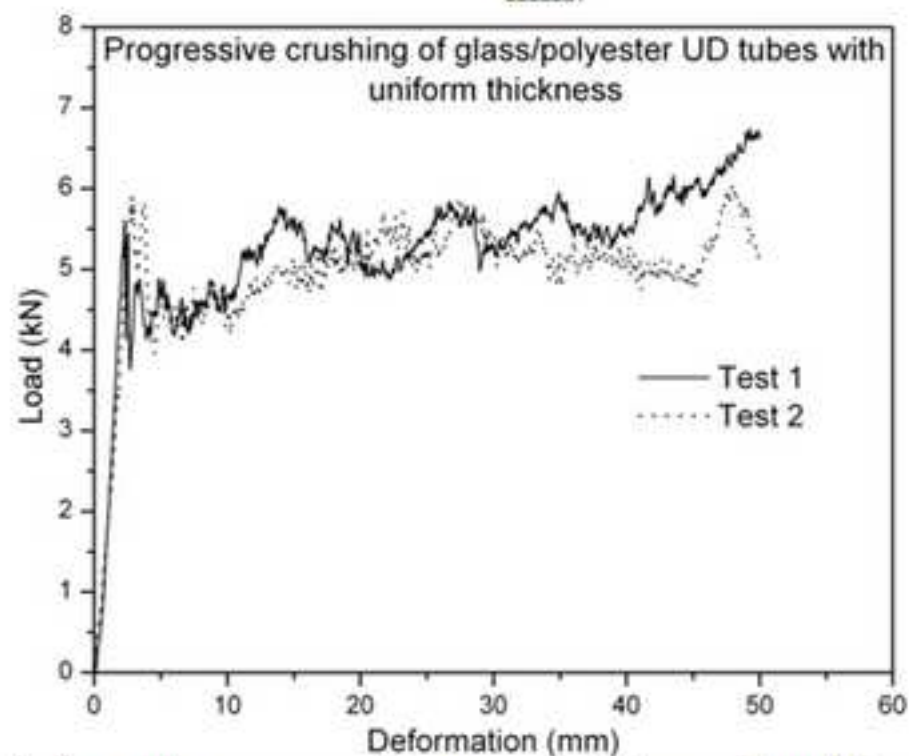


Figure 18

[Click here to download high resolution image](#)



(a) Progressive failure modes of composite tubes with uniform thickness of 1 mm.



(b) Load-deformation curves of composite tubes with uniform thickness of 1 mm.



(a)



(b)



(a)



(b)



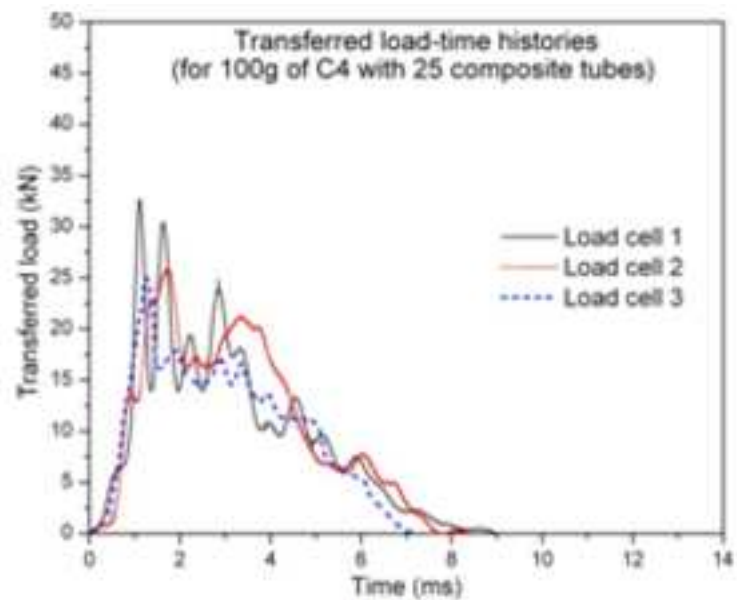
(c)



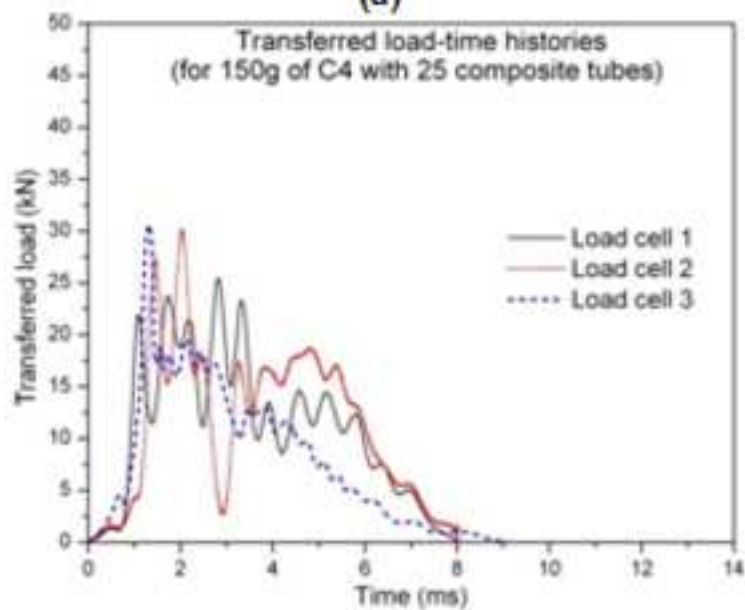
(d)

Figure 21

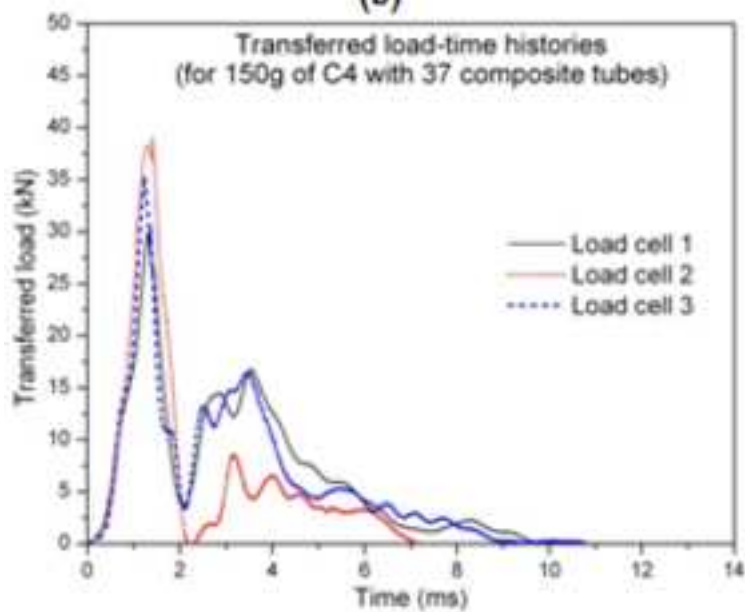
[Click here to download high resolution image](#)



(a)



(b)



(c)

Figure 22
[Click here to download high resolution image](#)

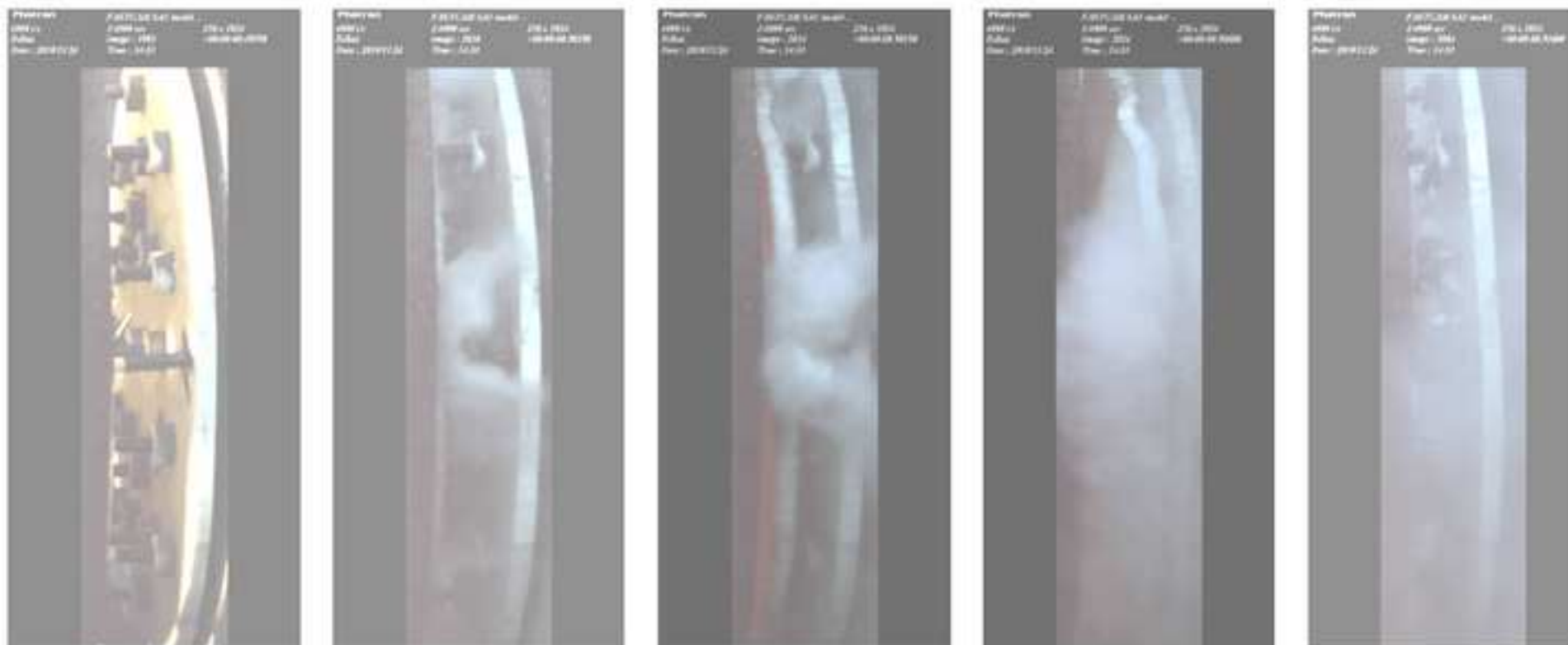


Figure 23

[Click here to download high resolution image](#)

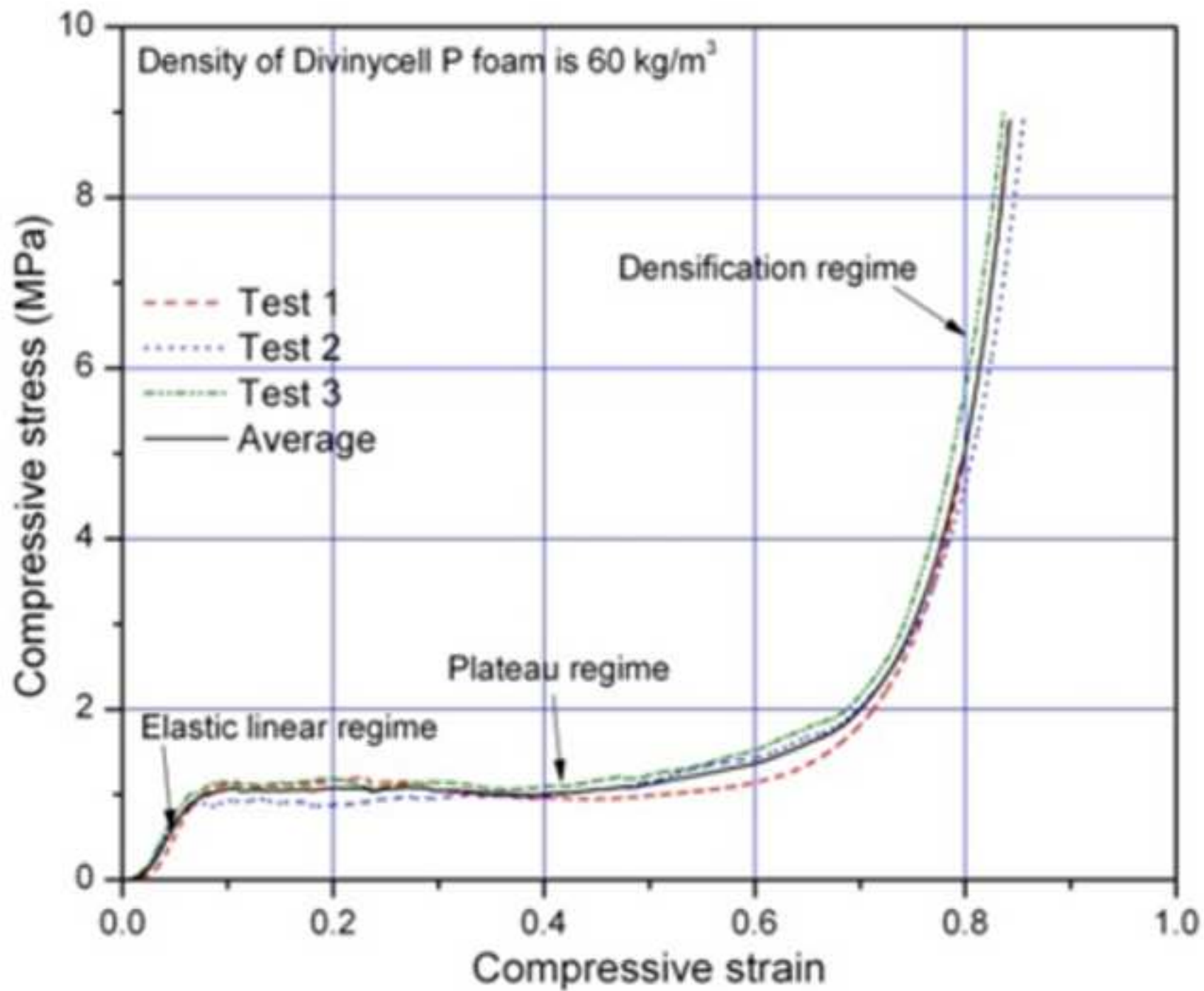
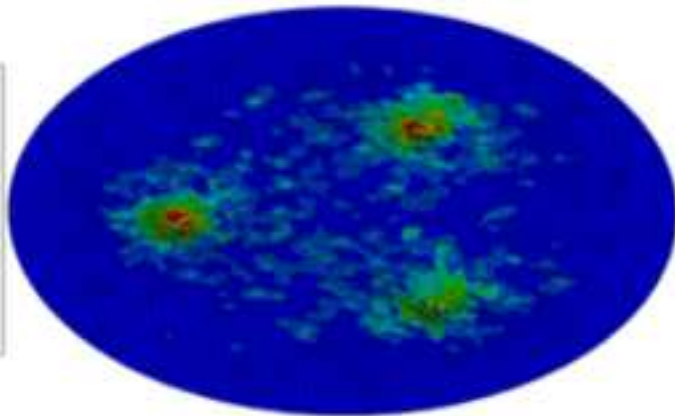
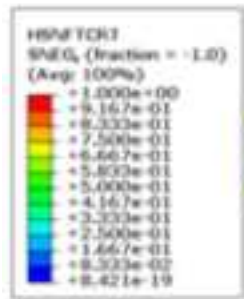
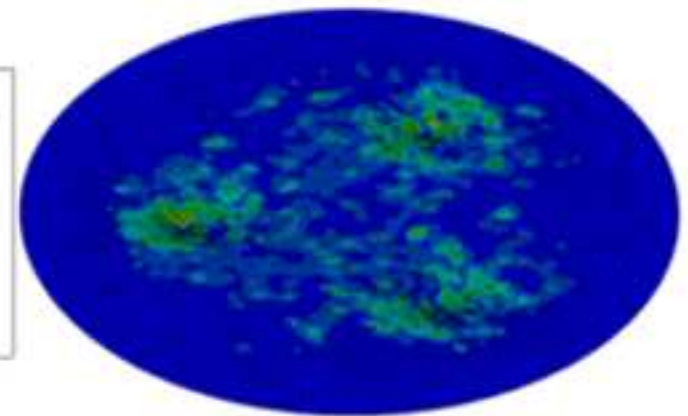
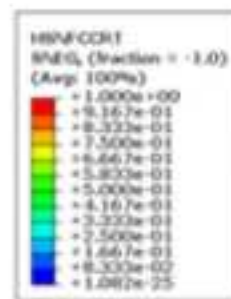


Figure 24

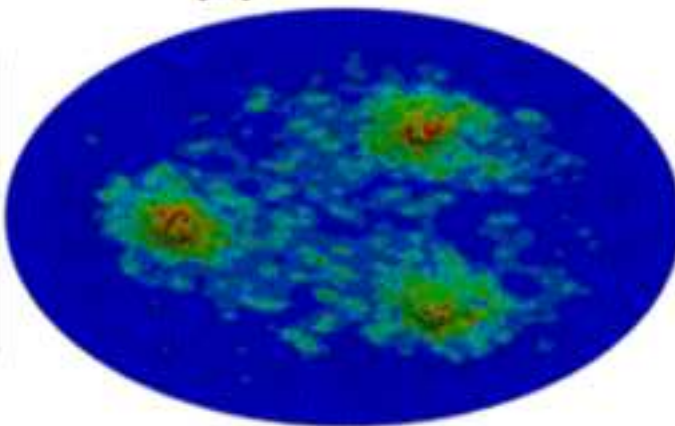
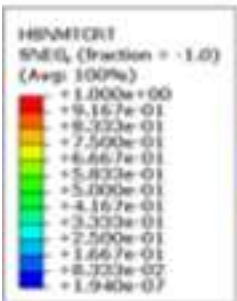
[Click here to download high resolution image](#)



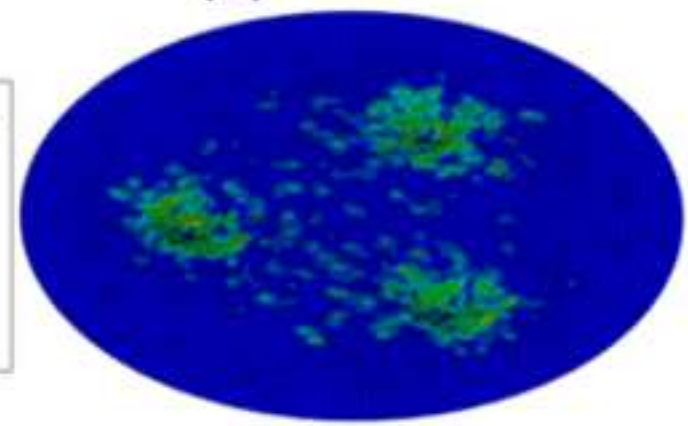
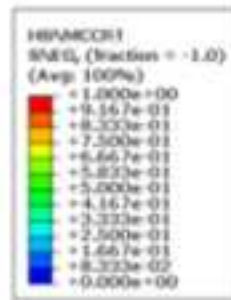
(a)



(b)



(c)



(d)

Figure 25

[Click here to download high resolution image](#)

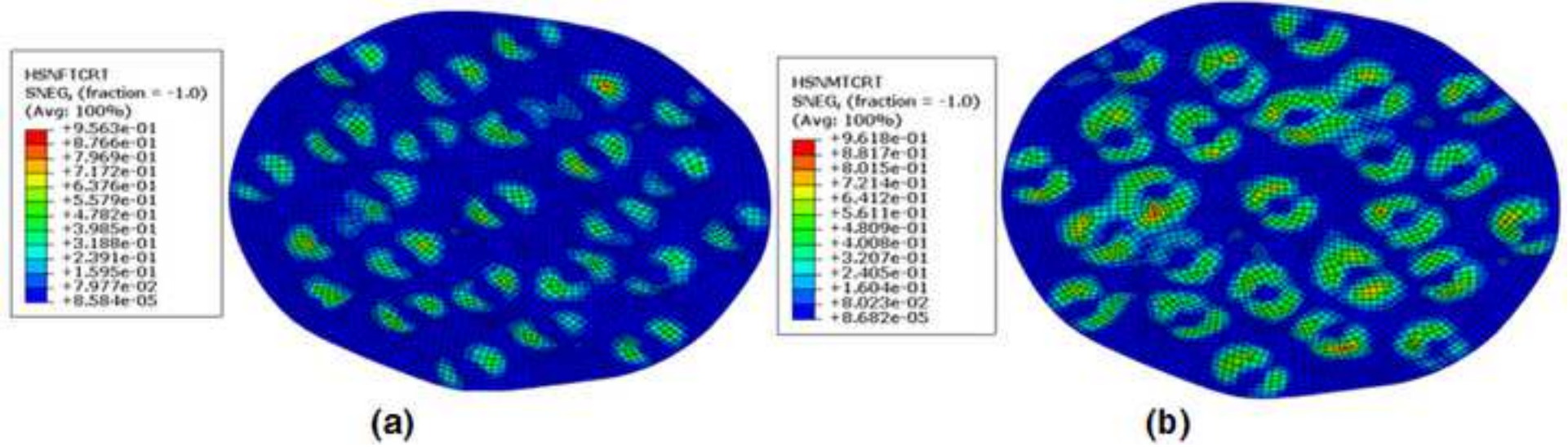


Figure 26

[Click here to download high resolution image](#)

